

We are IntechOpen, the world's leading publisher of Open Access books Built by scientists, for scientists

6,900

Open access books available

186,000

International authors and editors

200M

Downloads

Our authors are among the

154

Countries delivered to

TOP 1%

most cited scientists

12.2%

Contributors from top 500 universities



WEB OF SCIENCE™

Selection of our books indexed in the Book Citation Index
in Web of Science™ Core Collection (BKCI)

Interested in publishing with us?
Contact book.department@intechopen.com

Numbers displayed above are based on latest data collected.
For more information visit www.intechopen.com



Wavelet-based techniques in MRS

A. Suvichakorn^{a,*}, H. Ratiney^b, S. Cavassila^{b,†} and J.-P. Antoine^{a,‡}

^a*Institut de physique théorique (FYMA),
Université catholique de Louvain, B-1348 Louvain-la-Neuve, Belgium*

^b*CREATIS-LRMN, CNRS UMR 5220, Villeurbanne F-69621
Inserm, U630, Villeurbanne F-69621; INSA-Lyon, Villeurbanne F-69621
Université de Lyon, Lyon, F-69003; Université Lyon 1, Villeurbanne F-69622
France*

1. Introduction: magnetic resonance spectroscopic (MRS) signals

A magnetic resonance spectroscopic (MRS) signal is made of several frequencies typical of the active nuclei and their chemical environments. The amplitude of these contributions in the time domain depends on the amount of those nuclei, which is then related to the concentration of the substance (Hornak, 1997).

This property is exploited in many applications of MRS, in particular in the clinical one. The MRS spectra contain a wealth of biochemical information characterizing the molecular content of living tissues (Govindaraju et al., 2000). Therefore, MRS is a unique non-invasive tool for monitoring human brain tumours, etc. (Devos et al., 2004), if it is well quantified.

When an MRS proton signal is acquired at short echo-time (TE), the distortion of spectral multiplets due to J-evolution can be minimized and the signals are minimally affected by transverse relaxation. Such signals exhibit many more metabolite contributions, such as glutamate and myo-inositol, compared to long TE spectra. Therefore, an MRS signal acquired at short TE presents rich *in vivo* metabolic information through complicated, overlapping spectral signatures. However, it is usually contaminated by water residue and a baseline which mainly originates from large molecules, known as macromolecules. As the shape and intensity of the baseline are not known *a priori*, this contribution becomes one of the major obstructions to accurately quantify the overlapping signals from the metabolites, especially by peak integration, which is commonly used in frequency-based quantification techniques. Also, by seeing only the frequency aspect, one loses all information about time localization.

A number of quantification techniques have been proposed, which work either in the time domain (see Vanhamme et al. (2001) for a review) or in the frequency domain (see Mierisová & Ala-Korpela (2001) for a review). The time-domain based methods are divided into two main classes: on one side, non-interactive methods such as SVD-based methods (Pijnappel et al., 1992) and, on the other side, methods based on iterative model function fitting using strong prior knowledge such as QUEST (Ratiney et al., 2004; 2005), LCModel (Provencher, 1993), AQSES (Pouillet et al., 2007), or AMARES (Vanhamme et al., 1997).

*A. Suvichakorn is a Marie-Curie Research Fellow in the FAST (Advanced Signal Processing for Ultrafast Magnetic Resonance) Marie-Curie Research Network (MRTN-CT-2006-035801, <http://fast-mrs.eu>)

[†]E-mail address: Sophie.Cavassila@univ-lyon1.fr

[‡]E-mail address: Jean-Pierre.Antoine@uclouvain.be

However, there also exist techniques that analyse a signal in the two domains simultaneously and are therefore more efficient than, say, the Fourier transform, which gives only spectral information. The result is a time-scale and or a time-frequency representation, such as provided by the wavelet transform (WT) and the Short-Time Fourier transform (STFT). In addition, both transforms are local, in the sense that a small perturbation of a signal which may occur during the data acquisition will result only in a small, local modification of the transform.

A number of wavelet-based techniques have been proposed for spectral line estimation in MRS, including the continuous wavelet transform (Delprat et al., 1992; Guillemain et al., 1992; Serrai et al., 1997) and the wavelet packet decomposition (Mainardi et al., 2002). Among the various possibilities, we will concentrate our discussion on the continuous wavelet transform (CWT) with the Morlet wavelet (MWT). All wavelet calculations have been performed by our own wavelet toolbox, called YAWTb (Jacques et al., 2007). Some of the experimental aspects have been reported in Suvichakorn et al. (2009). For the convenience of the reader we have collected in the Appendix the basic features and properties of the CWT.

In the following sections, we will study the performance of the Morlet WT to retrieve parameters of interest such as resonances frequencies, amplitude and damping factors, for nuisances or impairments generally encountered in *in vivo* MRS signals: noise, baseline, solvent, and non-Lorentzian lineshapes.

2. The Morlet wavelet transform

The wavelet transform (WT) of a signal $s(t)$ with respect to a basic wavelet $g(t)$ is

$$\begin{aligned} S(\tau, a) &= \frac{1}{\sqrt{a}} \int g\left(\frac{t-\tau}{a}\right) s(t) dt \\ &= \frac{1}{2\pi} \sqrt{a} \int \overline{G(a\omega)} S(\omega) e^{i\omega\tau} d\omega, \end{aligned} \quad (1)$$

where $S(\omega)$ is the Fourier transform of the signal, $a > 0$ is a dilation parameter that characterizes the frequency of the signal (since $1/a$ is essentially a frequency), $\tau \in \mathbb{R}$ is a translation parameter that indicates the localization in time and $\overline{G(a\omega)}$ is the complex conjugate of the (scaled) Fourier transform of $g(t)$. We can think of the basic wavelet as a window which slides through the signal, giving the information at instantaneous time τ . The window is also dilated by a , so that a small a corresponds to a high frequency of the signal, and *vice versa*. As a result, the WT becomes a function of both time and frequency (scale). For more details, see the Appendix.

A technique based on the continuous wavelet transform (CWT) was proposed by Guillemain et al. (1992). By exploiting the ability of the CWT to see the information in the two domains simultaneously, it can extract the information from MRS signals directly without any decomposition or pre-processing, in order to quantify an MRS signal. The technique proceeds in two steps: (i) detection of the frequency of the peaks in MRS signals and (ii) characterization at each detected frequency. It can be described as follows.

At a particular value of a , the WT $S_a(\tau) \equiv S(\tau, a)$ can be represented in terms of its modulus $|S_a(\tau)|$ and phase $\Phi_a(\tau)$, namely,

$$S_a(\tau) = |S_a(\tau)| e^{i\Phi_a(\tau)}, \quad (2)$$

with an instantaneous frequency

$$\begin{aligned}\Omega_a(\tau) &= \frac{\partial}{\partial \tau} \Phi_a(\tau) \\ &= \frac{\partial}{\partial \tau} \text{Im}[\ln S_a(\tau)] \\ &= \text{Im} \left[\frac{1}{S_a(\tau)} \frac{d}{d\tau} S_a(\tau) \right],\end{aligned}\quad (3)$$

Next, let us consider an MRS signal with a Lorentzian damping function, namely,

$$s_L(t) = Ae^{-Dt} e^{i(\omega_s t + \varphi)} \Leftrightarrow S_L(\omega) = 2\pi A e^{i\varphi} \delta(\omega - (\omega_s + iD)), \quad (4)$$

where D and φ denote the damping factor and the phase of the signal. Its WT is accordingly

$$\begin{aligned}S_L(\tau, a) &= \sqrt{a} A e^{i\varphi} e^{-D\tau} e^{i\omega_s \tau} \overline{G(a(\omega_s + iD))} \\ &= \sqrt{a} s(\tau) \overline{G(a(\omega_s + iD))}.\end{aligned}\quad (5)$$

For a Morlet function scaled by a dilation parameter a (we omit the negligible correction term, see Eq.(A.9)), namely,

$$G_M(a\omega) = \exp\left(-\frac{1}{2}\sigma^2(a\omega - \omega_0)^2\right), \quad (6)$$

it can be seen that the modulus of $S(\tau, a)$ is maximum, i.e., $\frac{\partial}{\partial a} S(\tau, a) \rightarrow 0$, when $\frac{\partial}{\partial a} G \rightarrow 0$. Given that $a > 0$ and the assumption that $\omega_s \gg D$, the maximum can be found along the scale $a_r = \omega_0 / \omega_s$ (this is called a *horizontal ridge*), which then gives

$$\overline{G_M(a_r(\omega_s + iD))} = \exp\left(\left(\frac{\sigma a_r D}{\sqrt{2}}\right)^2\right), \quad (7)$$

and consequently

$$S_{a_r}(\tau) = \sqrt{a_r} \exp\left(\left(\frac{\sigma a_r D}{\sqrt{2}}\right)^2\right) s(\tau), \quad (8)$$

which is identical to the signal $s(t)$ multiplied by a coefficient depending on the still unknown D . Consider the modulus of the Morlet wavelet transform (MWT) along a_r ,

$$\begin{aligned}|S_{a_r}(\tau)| &= \sqrt{a_r} \exp\left(\left(\frac{\sigma a_r D}{\sqrt{2}}\right)^2\right) |s(\tau)| \\ \ln |S_{a_r}(\tau)| &= \frac{1}{2} \ln a + \left(\frac{\sigma a_r D}{\sqrt{2}}\right)^2 + \ln A - D\tau.\end{aligned}\quad (9)$$

That is,

$$D = -\frac{\partial}{\partial \tau} \ln |S_{a_r}(\tau)|. \quad (10)$$

Knowing D can now lead to the estimation of the amplitude resonance A of the signal by

$$A = |s(t)| e^{Dt}. \quad (11)$$

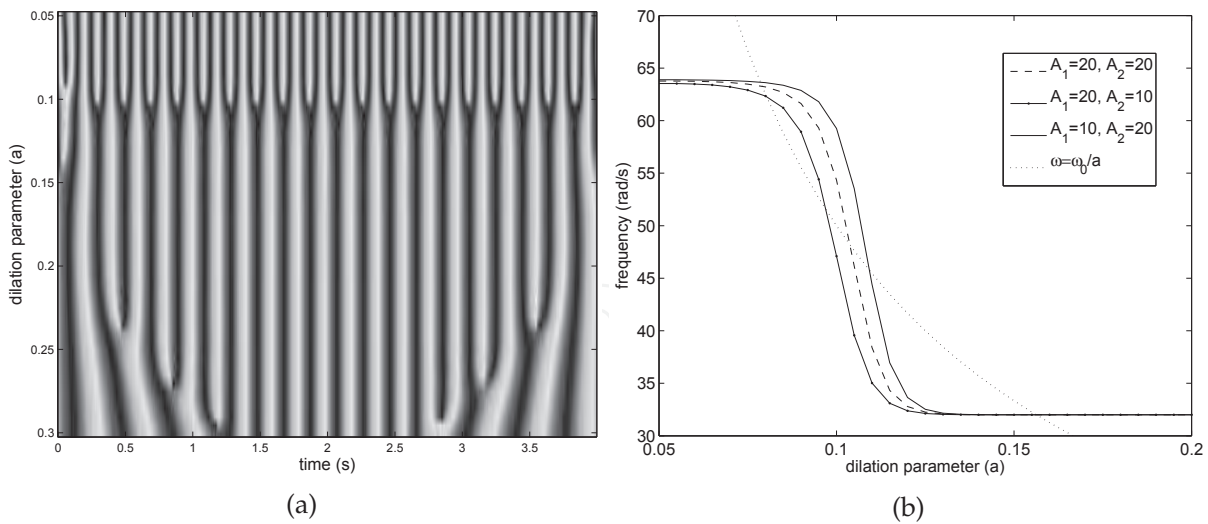


Fig. 1. (a) Phase of the Morlet wavelet transform of a signal $s(t)$ containing two frequencies $\omega_s=32$ and 64 rad/s and (b) its instantaneous frequency. Here $\sigma = 1$, $\omega_0 = 5$ rad/s, sampling frequency $F_s = 256$ s $^{-1}$, data length $l = 1024$ points.

Since $S_{a_r}(\tau)$ is a function of time, the derived D is also a function of time. This is beneficial for analysing signals that do not have a steady damping function. In addition, considering the phase of the MWT along a_r , namely,

$$\arg S_{a_r}(\tau) = \omega_s \tau + \varphi,$$

we also have

$$\begin{aligned} \omega_s &= \frac{\partial}{\partial \tau} \arg S_{a_r}(\tau) \\ &= \Omega_{a_r}(\tau), \end{aligned} \quad (12)$$

as in Eq.(3). Strictly speaking, the instantaneous frequency at the scale a_r of the Morlet transform is ω_s . This can be observed in Figure 1, which shows that the instantaneous frequency intersects the line ω_0/a at $a = \omega_0/\omega_s$, where $\omega_s=32$ and 64 rad/s are the frequencies of the signal. The phase of the signal $\varphi \in (-\pi, \pi)$ can also be derived from the phase of the WT, if needed. The property given in Eq.(12) is useful for analysing an n -frequency signal; it indicates the actual frequencies of the signal and the scale a that we should consider. In addition, if its frequencies are sufficiently far away from each other, so that $\overline{G(a\omega)}$ treats each spectral line independently (Barache et al., 1997), the amplitude at each frequency can thus be derived. When two frequencies are very close to each other (this also depends on the sampling frequency), increasing the frequency of the Morlet function ω_0 can better localize and distinguish the overlapping frequencies. On the other hand, ω_s can be obtained iteratively by

1. Initializing $a = a_i$ at some values.
2. Calculating the instantaneous frequency, namely Ω_{a_i} .
3. Assigning the new value to $a_{i+1} = \omega_0/\Omega_{a_i}$.
4. Repeating the process until a converges to ω_s .

Figure 2 illustrates an overlap of two frequencies and the derived instantaneous frequencies using the iteration method. The derived frequencies converge to the true frequencies within a few steps.

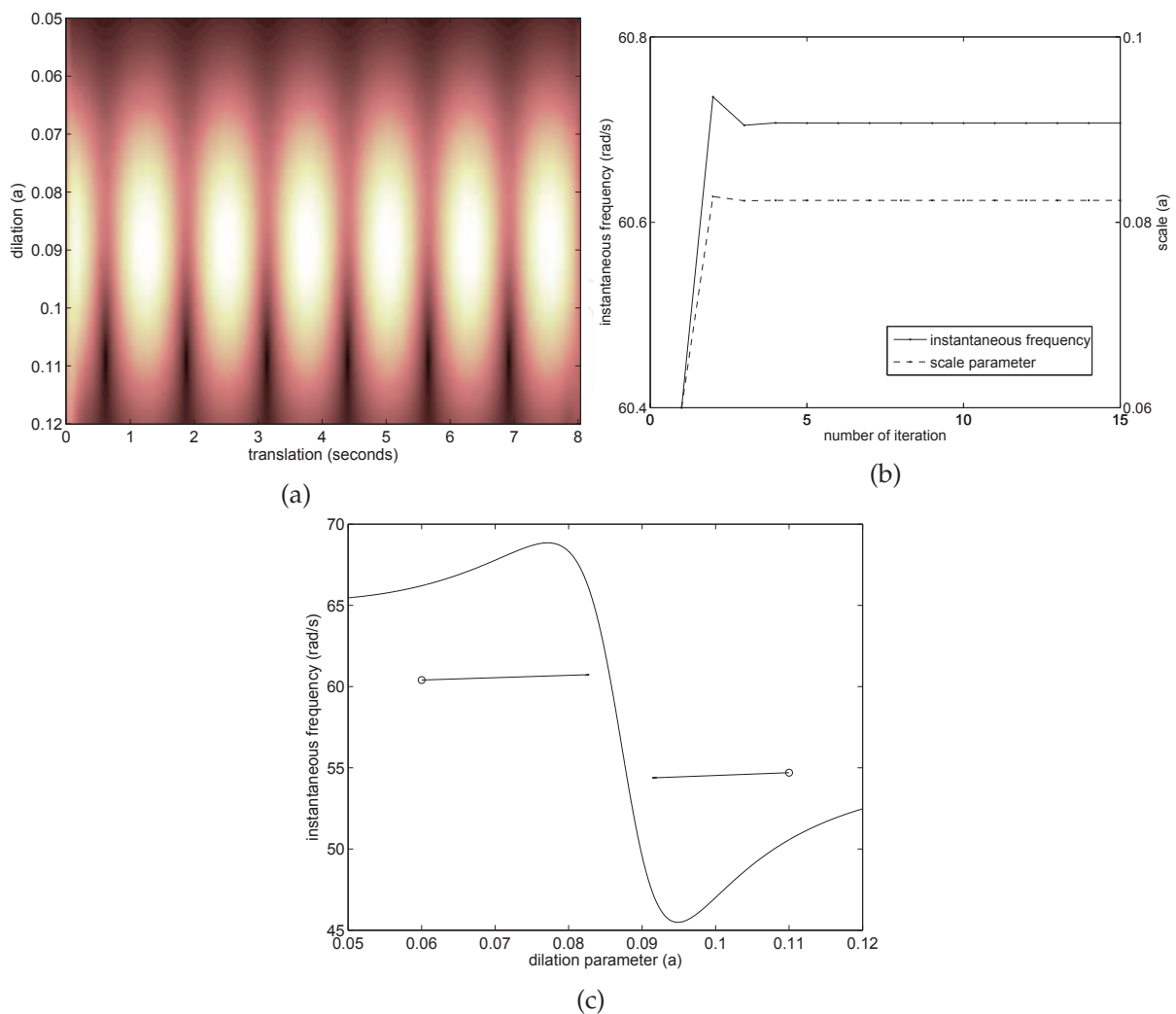


Fig. 2. (a) The MWT of $y(t) = \exp(i55t) + \exp(i60t)$ and (b) its instantaneous frequencies when using the iterative method. Here $\sigma = 1$, $\omega_0 = 5.5 \text{ rad/s}$, $F_s = 800 \text{ s}^{-1}$, $l = 1024$ points. (c) Comparison of the instantaneous frequencies by the non-iterative and the iterative method. The symbol \circ indicates an initial value of a .

3. Continuous Wavelet Transform and the *in vivo* MRS challenges

3.1 Gaussian White Noise

An *in vivo* MRS signal is always impaired by additive noise, which is usually assumed to be white gaussian. This noise causes oscillations in the instantaneous frequency derived with the CWT representation, as illustrated in Figure 3 which shows the instantaneous frequency derived from a signal with a peak at a frequency of 32 rad/s with an additive Gaussian noise corresponding to a signal to noise ratio (SNR) of 10.¹ In order to reduce this effect, Guillemain

¹ The Signal to Noise ratio SNR is defined as the ratio of the time domain first point amplitude of the resonance to the time domain noise standard deviation

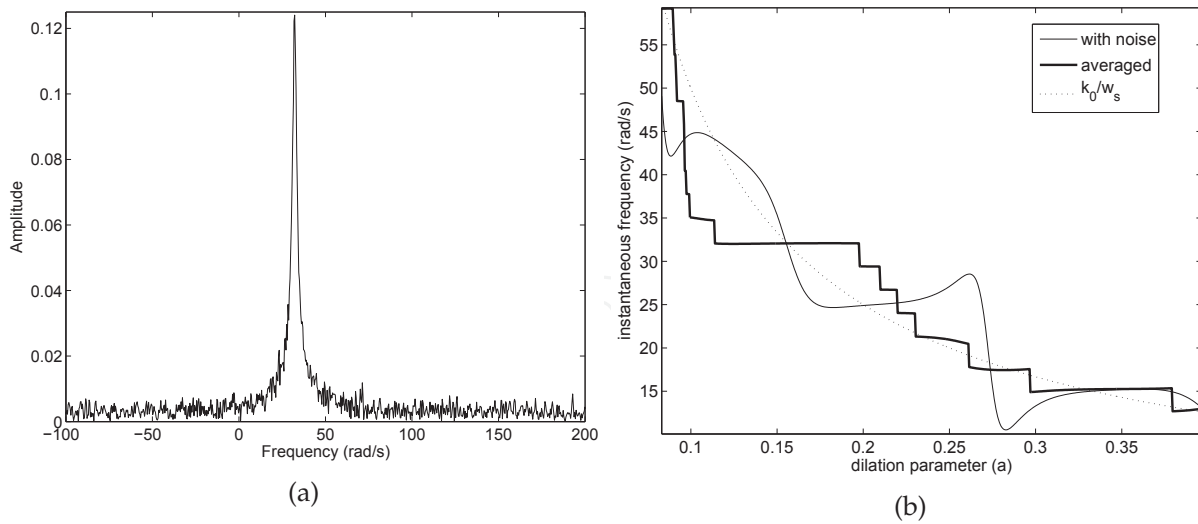


Fig. 3. (a) A spectrum with one resonance at 32 rad/s with SNR=10 ($\sigma_n = 0.079$) and (b) its instantaneous frequency derived by the Morlet wavelet at $t = 4.7$ s ($\omega_0 = 5$ rad/s, $\sigma=1$, $F_s = 800$ s⁻¹).

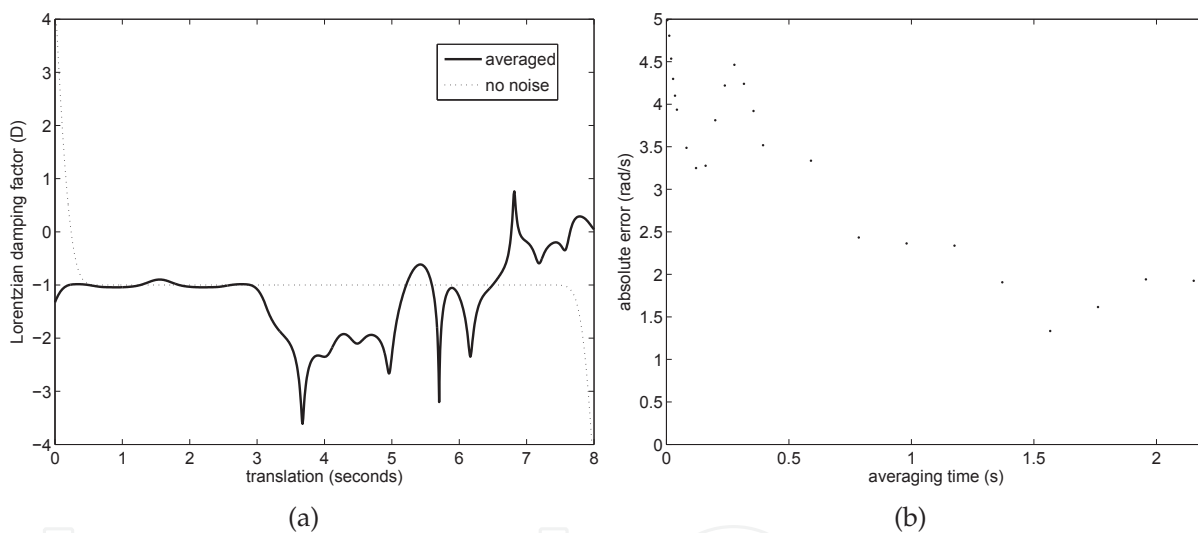


Fig. 4. For the signal shown in Figure 3(a): Derived Lorentzian damping factor and (b) absolute frequency estimation error with respect to the averaging time, calculated at the scale $a = \omega_0/\omega_s$ of the Morlet wavelet transform (SNR = 10, $\omega_s = 32$ rad/s, $\omega_0 = 5$ rad/s, $\sigma = 1$, $F_s = 800$ s⁻¹).

et al. (1992) suggested averaging in time the derived parameters, for instance $\Omega_a(\tau)$, i.e.,

$$\bar{\Omega}_a = \frac{1}{T} \int_{\tau_0}^{\tau_0+T} \Omega_a(\tau) d\tau. \tag{13}$$

As can be seen in Figure 3, averaging in time reduces the noise effect on the derivation of the instantaneous frequency.² One can see that averaging creates many steady points. At the scale $a = \omega_0/32$, the instantaneous frequency is about, but not exactly, 32 rad/s. Here, the

² This property might be used for denoising, but this has not been exploited.

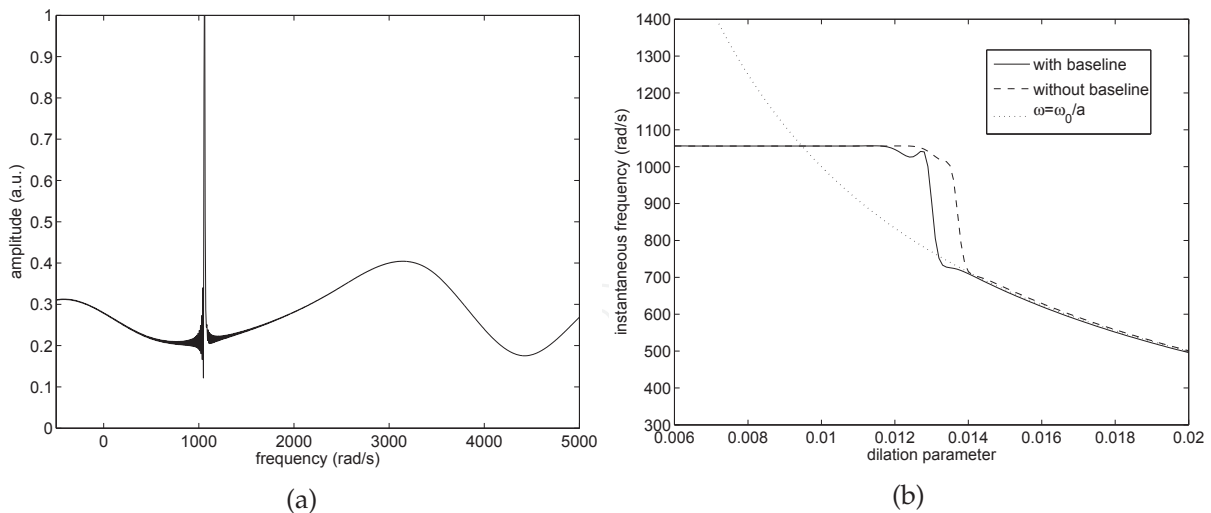


Fig. 5. (a) The Fourier transform of a 1056-rad/s signal with baseline; b) Its instantaneous frequency ($\omega_0 = 10$ rad/s, $\sigma = 1$). The baseline is modelled by a cubic spline.

averaging time is 1.56 s. Figure 4(b) shows the evolution of the absolute frequency estimation with respect to the averaging time. Increasing the averaging time is likely to decrease the estimation error, as illustrated in Figure 4(b). The same approach can be used to derive the instantaneous damping factor. The estimated instantaneous damping factor is also smoother and closer to the actual damping factor when time averaging is employed. Although the method described above should work at any value of a , there is a particular range of a that is meaningful, and should be wisely selected. As a rule of thumb, this range should not be far from the scale that maximizes the modulus of the Morlet WT.

3.2 Baseline

The baseline corresponds to contributions from large molecules, with a broad frequency pattern in the MRS spectrum. Thus, it becomes a major obstruction in the quantification of metabolite contribution from the MRS signals. First, we simulate the baseline by cubic splines in order to study the performance of the MWT when a baseline is present. In the case of Figure 5, the simulated baseline has no effect on the instantaneous frequency derived from the WT. Then, we used a baseline modelled with 50 randomly distributed Lorentzian profiles with a large damping factor, compared to the signal-of-interest at 3447 rad/s, e.g. $s_L(t) = \exp(-10t) \exp(i3447t) + B(t)$ where $B(t) = \exp(-50t)[0.2 \exp(i3447t) + 0.3 \exp(i2000t) + \dots]$ is the baseline (see Figure 6). The first component of $B(t)$ has the same frequency as the signal, in order to imitate the overlap between the baseline and the signal. It is found that the modelled baseline does not prevent an accurate estimation of both the damping factor and the amplitude derived from the Morlet WT, provided one waits until both the effect of the baseline and the edge effect (discussed in Section 4.1 below) have died out. In the example shown here, the waiting time is approximately 0.2 s.

The MWT in Figure 6(b) tells us that the baseline affects only the beginning of the transform in the time (τ) axis, comparing to the long, clear peak of our 3447-rad/s signal. This means that the baseline can be assumed to decay faster than the pure signal, and the method described should still be effective without removing the baseline beforehand. Such an assumption has been widely used in spectroscopic signal processing, where several authors have proposed truncation of the initial data points in the time domain, which are believed to contain a major

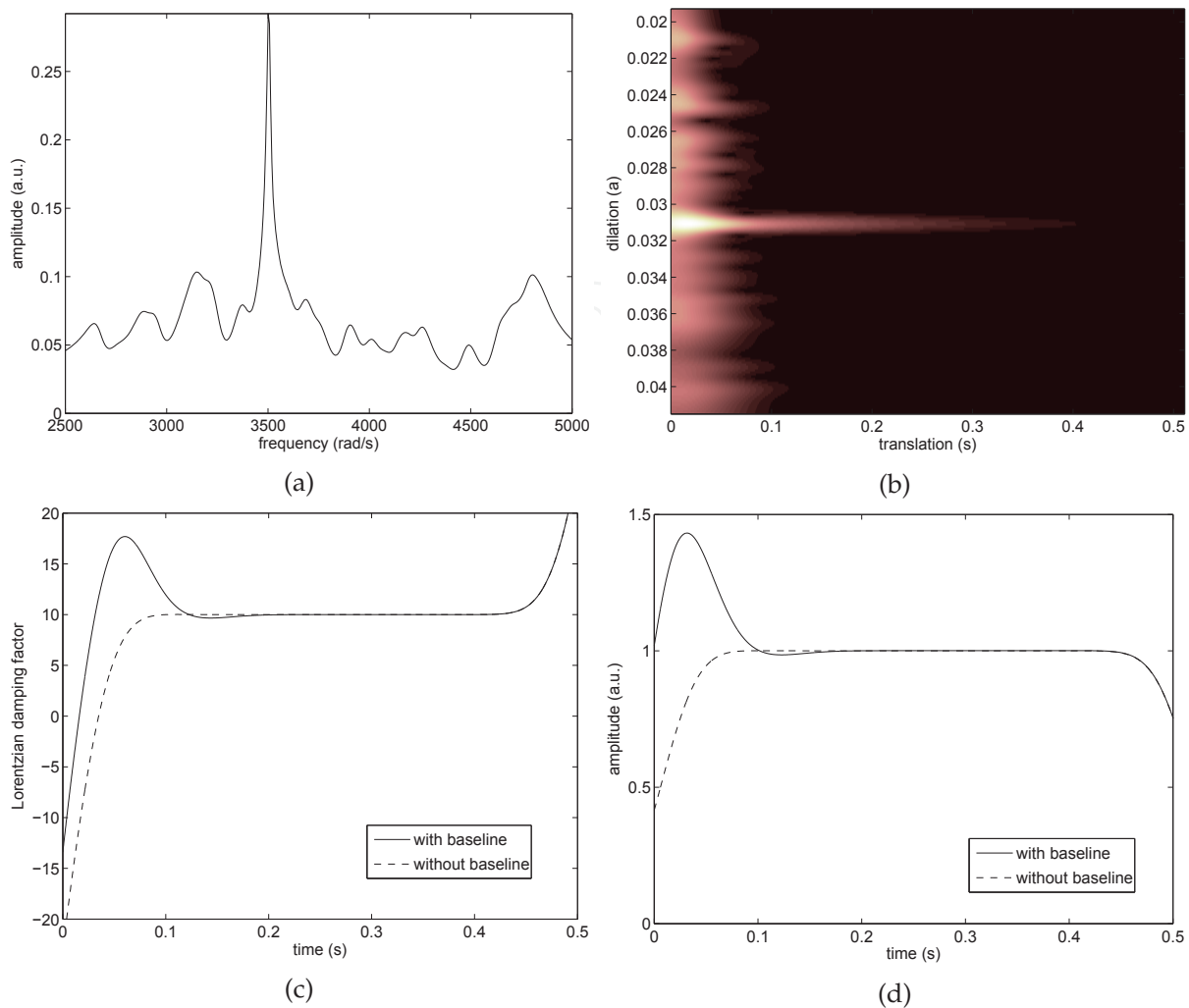


Fig. 6. (a) The Fourier transform of a 3447-rad/s Lorentzian signal with baseline. The latter is modelled by large Lorentzian damping factors; (b) Its Morlet WT and the derived parameters: (c) damping factor and (d) amplitude. The actual parameters are 10 s^{-1} and 1 a.u. for the damping factor and amplitude, respectively. ($\omega_0 = 100 \text{ rad/s}$, $\sigma = 1$). From Suvichakorn et al. (2009).

part of the baseline. However, some information of the metabolites could be lost and a strategy for properly selecting the number of data points is needed (see Rabeson et al. (2006) for examples and further references).

Next, in order to study the characteristics of the real baseline by the Morlet wavelet, an *in vivo* macromolecule MRS signal was acquired on a horizontal 4.7T Biospec system (BRUKER BioSpin MRI, Germany). The data acquisition was done using the differences in spin-lattice relaxation times (T1) between low molecular weight metabolites and macromolecules (Behar et al., 1994; Cudalbu et al., 2009; 2007).

As seen in Figure 7, the metabolite-nullified signal from a volume-of-interest (VOI) central-

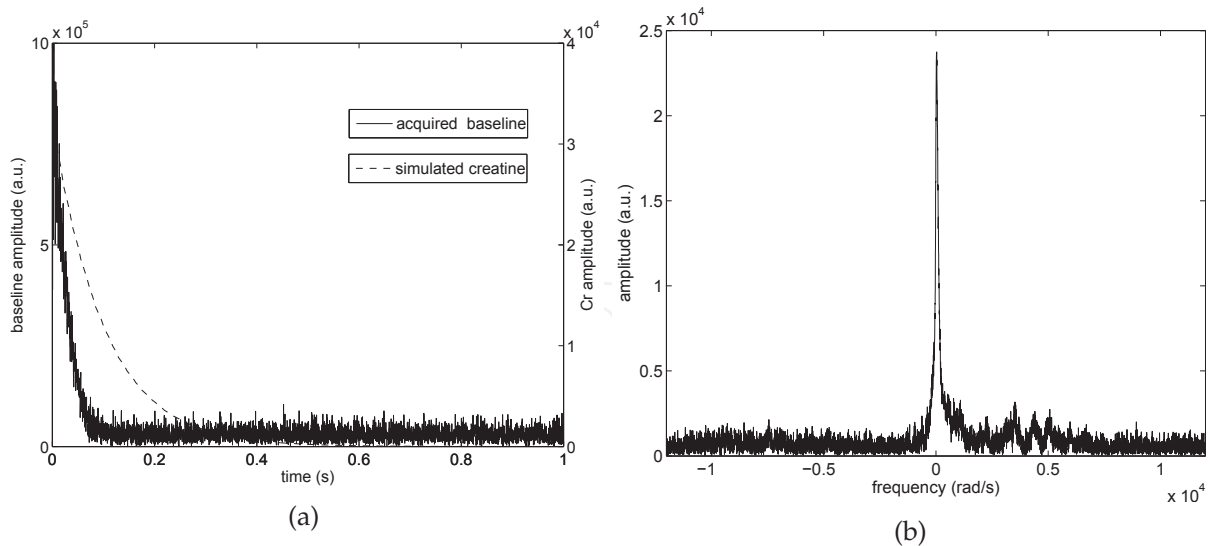


Fig. 7. (a) The signal of baseline + residual water (a) in time domain; and (b) in frequency domain.

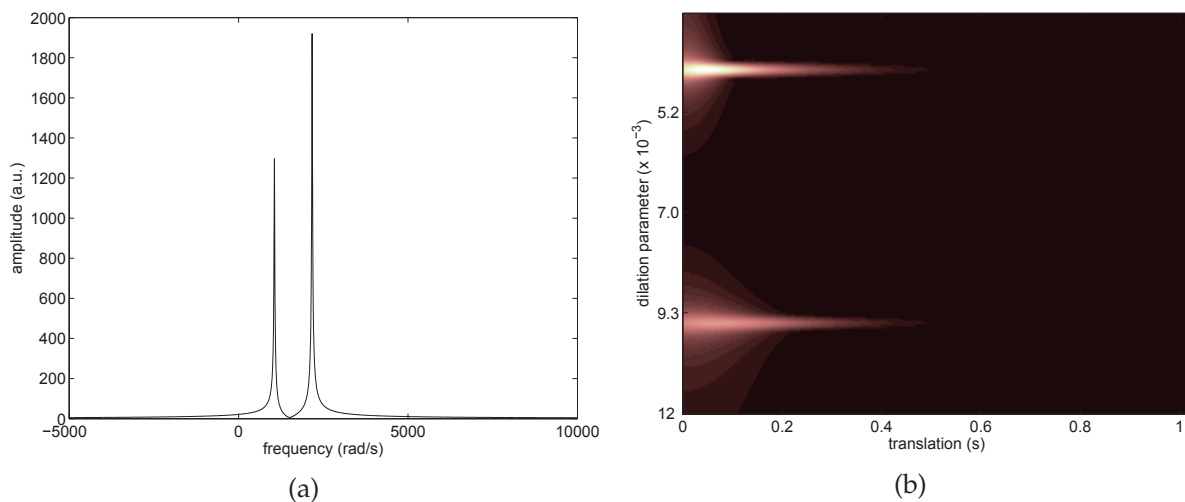


Fig. 8. (a) Frequency response of creatine at 4.7 Tesla and (b) its Morlet WT ($\omega_0 = 10 \text{ rad/s}$, $\sigma = 1$, $F_s = 4006.41 \text{ s}^{-1}$). The parameters derived from the Morlet transform are $D = 10 \text{ s}^{-1}$, $\omega_1 = 1056 \text{ rad/s}$, $A_1 = 1330 \text{ a.u.}$ and $\omega_2 = 2168 \text{ rad/s}$, $A_1 = 1965 \text{ a.u.}$

ized in the hippocampus of a healthy mouse³ resulted from a combination of residual water, baseline and noise. Compared to the simulated signal of creatine, whose frequency response and Morlet WT are shown in Figure 8, the signal decays much faster, making it suitable to use the Morlet wavelet to analyse the MRS signal as described earlier. For studying this, the two signals are normalised to the same amplitude and added together. Then the amplitude of the

³ An Inversion-Recovery module was included prior to the PRESS sequence (echo-time = 20ms, repetition time = 3.5s, bandwidth of 4kHz, 4096 data-points) in order to measure the metabolite-nullified signal. The water signal was suppressed by variable power RF pulses with optimized relaxation delays (VAPOR). All first- and second-order shimming terms were adjusted using the Fast, Automatic Shimming technique by Mapping Along Projections (FASTMAP) for each VOI ($3 \times 3 \times 3 \text{ mm}^3$). Inversion time = 700 ms.

creatine is derived with the Morlet WT. Next, we multiply the simulated, normalised creatine by 0.5, 1, 1.5, . . . For each of these values, we derive the amplitude and plot the result in Figure 9. The recovery of the (simulated) creatine at different amplitudes, after adding it to the baseline signal, reveals that the amplitude of the metabolite can be correctly derived using $t = 0.4$ s, whereas at earlier time ($t < 0.2$ s) the derived amplitude still suffers from the boundary effect (we will discuss this effect in Section 4.1). However, the metabolite signal is covered later by noise ($t = 0.77$ s), giving an inaccurate amplitude estimate. Therefore, the time to monitor the amplitude of the metabolite should be properly selected. Another data set of the baseline⁴ acquired at 9.4T, with a better signal to noise ratio and a better water suppression, shows similar characteristics (see Figure 10).

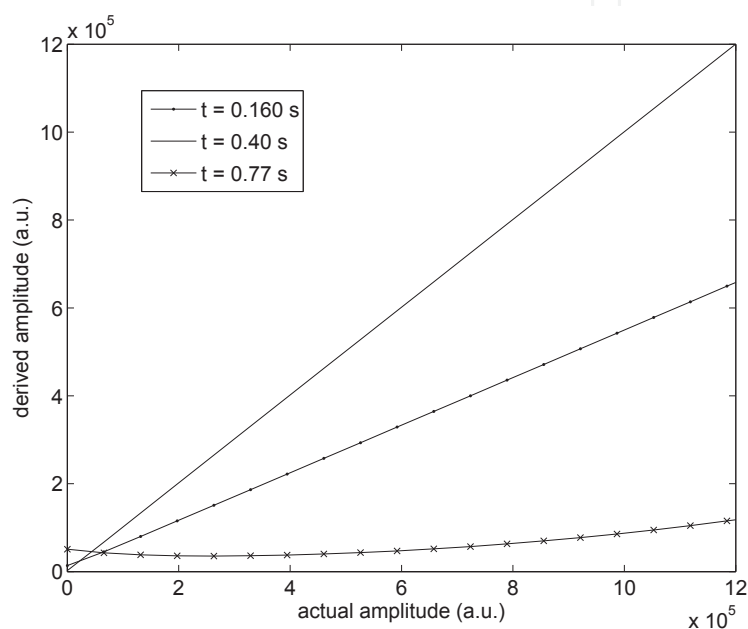


Fig. 9. Derived amplitude at $\omega = 1056$ rad/s, using $\omega_0 = 100$ rad/s and $\sigma = 1$ from a signal containing a simulated creatine signal and an *in vivo* acquired macromolecule signal.

3.3 Solvent

In MRS quantification, a large resonance from the solvent needs to be suppressed to unveil the metabolites without altering their magnitudes. The intensity of the solvent is usually several orders of magnitude larger than those of the metabolites.

⁴ received from Cristina Cubaldu, Laboratory for Functional and Metabolic Imaging (LIFMET), Ecole Polytechnique Fédérale de Lausanne (EPFL).

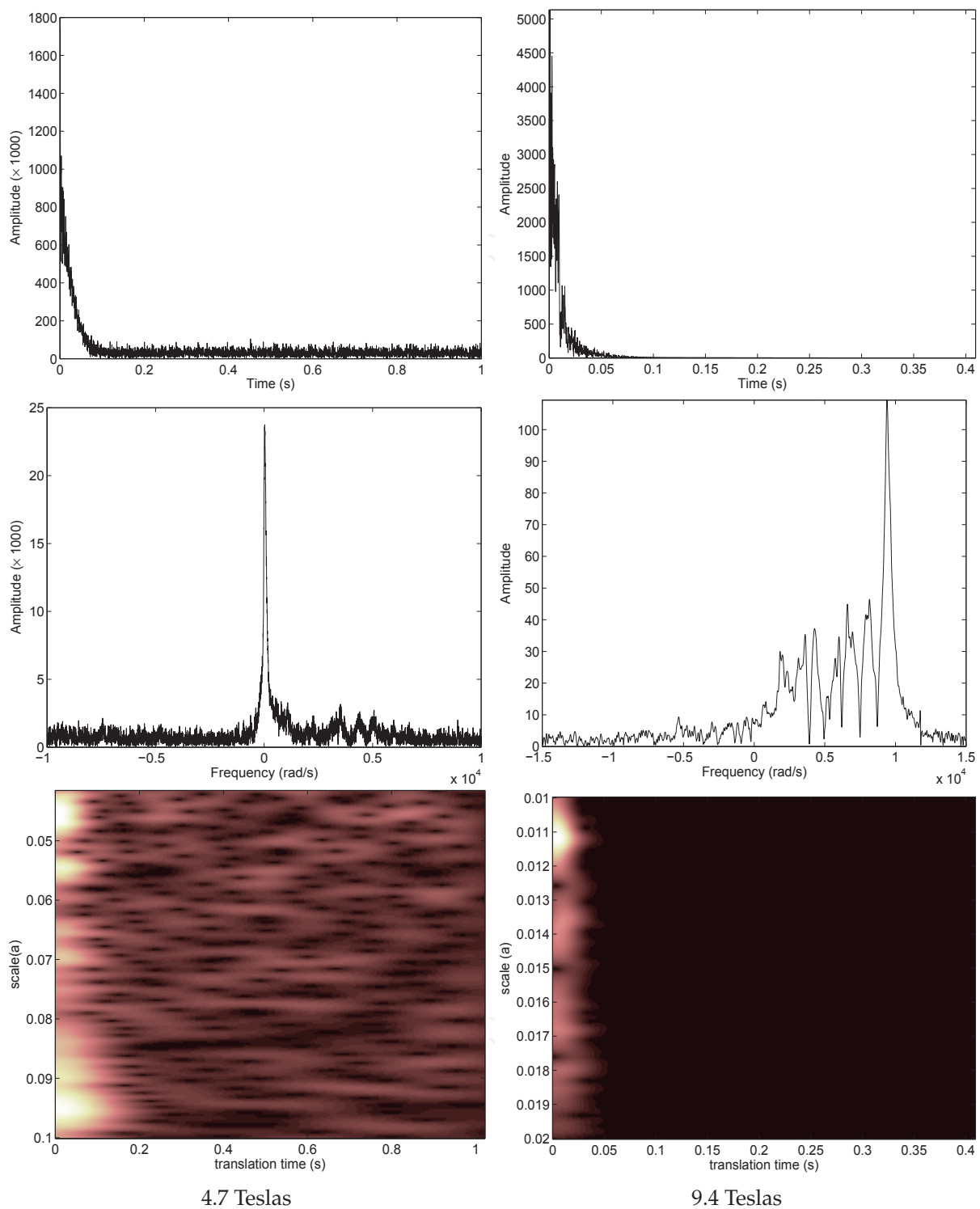


Fig. 10. Macromolecules MRS signals acquired at 4.7 Teslas and 9.4 Teslas, respectively, their Fourier transforms and their Morlet WT.

The Morlet WT sees the signal at each frequency individually, therefore it can work well even if the amplitudes at various frequencies are hugely different, which normally occurs when there is a solvent peak in the signal. In order to illustrate this, the Morlet WT has been applied

to the following signal

$$s(t) = 100e^{-8.5t}e^{i32t} + e^{-1.5t}e^{i60t} + e^{-0.5t}e^{i90t} + e^{-t}e^{i120t} + e^{-2t}e^{i150t}, \quad (14)$$

as seen in Figure 11 (a). This signal has an amplitude of 100 at 32 rad/s and 1 elsewhere. The high amplitude can affect other frequencies if they are close to each other. This is illustrated in Figure 11 (b) when a Hann window is applied to the signal in order to separate each frequency. Using the aforementioned method, the amplitude of 1 is derived as 0.980, 0.911, 0.988 and 0.974 respectively. The error ranges within 1.2-8.9 %, without any preprocessing.

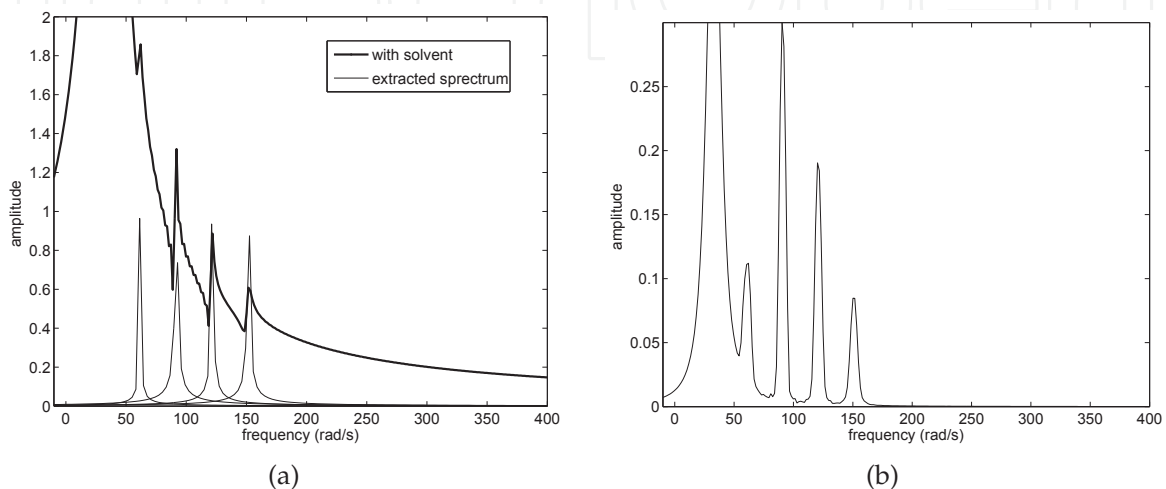


Fig. 11. (a) The Fourier transform of a signal with different amplitudes and the spectrum extracted by the Morlet wavelet and (b) by a Hann window.

3.4 Non-Lorentzian lineshape

The ideal Lorentzian lineshape assumes that the homogeneous broadening is equally contributed from each individual molecule. However, imperfect shimming and susceptibility effects from internal heterogeneity within tissues lead to non-Lorentzian lineshapes in real experiments (Cudalbu et al., 2008). These effects are typically modelled by a Gaussian lineshape (Franzen, 2002; Hornak, 1997). Since the inhomogeneous broadening is often significantly larger than the lifetime broadening, the Gaussian lineshape is often dominant. If the lineshape is intermediate between a Gaussian and a Lorentzian form, the spectrum can be fitted to a convolution of the two functions (Marshall et al., 2000; Ratiney et al., 2008). Such lineshape is known as a *Voigt profile*.

Next we will explore how the Morlet WT can deal with the Gaussian and Voigt lineshapes. Consider a pure Gaussian function modulated at the frequency ω_s , namely,

$$s_G(t) = Ae^{-\gamma t^2} e^{i\omega_s t}. \quad (15)$$

Its Morlet WT is

$$\begin{aligned} S_G(\tau, a) &= \frac{1}{\sqrt{a}} \int g_M\left(\frac{t-\tau}{a}\right) s_G(t) dt \\ &= \frac{A}{2\pi\sqrt{a}\sigma} \int e^{-\gamma t^2} e^{i\omega_s t} e^{-\left(\frac{t-\tau}{\sqrt{2}\sigma a}\right)^2} e^{-i\omega_0\left(\frac{t-\tau}{a}\right)} dt \\ &= \frac{A}{2\pi\sqrt{a}\sigma} \int e^{-(k_1 t^2 + k_2 t + k_3)} dt, \end{aligned} \quad (16)$$

where

$$\begin{aligned} k_1 &= \gamma + \frac{1}{2\sigma^2 a^2} \\ k_2 &= -i\left(\omega_s - \frac{\omega_0}{a}\right) - \frac{\tau}{\sigma^2 a^2} \\ k_3 &= -i\frac{\omega_0 \tau}{a} + \frac{\tau^2}{2\sigma^2 a^2}. \end{aligned}$$

Eq.(16) is known as a Gaussian integral and can be computed explicitly:

$$\int_{-\infty}^{\infty} e^{-(k_1 t^2 + k_2 t + k_3)} dt = \sqrt{\frac{\pi}{k_1}} e^{\frac{k_2^2}{4k_1} - k_3}. \quad (17)$$

As a result, the Morlet WT at the scale $a_r = \omega_0/\omega_s$ is

$$S_{G,a_r}(\tau) = k_4 A e^{-k_5 \tau^2} e^{i\omega_s \tau}, \quad (18)$$

where

$$\begin{aligned} k_4 &= \sqrt{\frac{a_r}{2\pi(2\gamma\sigma^2 a_r^2 + 1)}} \\ k_5 &= \frac{\gamma}{2\gamma\sigma^2 a_r^2 + 1}, \end{aligned}$$

which is also a Gaussian function at the frequency ω_s . The width and amplitude of this new Gaussian function are functions of ω_s and of the width of the original Gaussian signal $s_G(t)$. Therefore, similarly to the process of the Lorentzian lineshape, the amplitude (A) and the width of the Gaussian function (inversely proportional to γ) can be obtained as follows:

1. Find $\omega_s = \frac{\partial}{\partial \tau} \arg S_{G,a_r}(\tau)$.
2. Find γ from the second derivative of $\ln |S_{G,a_r}(\tau)|$, which yields

$$\gamma = -\frac{0.5}{\left(\frac{\partial^2}{\partial \tau^2} \ln |S_{G,a_r}(\tau)|\right)^{-1} + \sigma^2 a_r^2}. \quad (19)$$

3. Find A from the calculated ω_s and γ .

On the other hand, the Morlet WT at the scale $a_r = \omega_0/\omega_s$ of a Voigt lineshape,

$$s_V(t) = A e^{-\gamma t^2} e^{-Dt} e^{i\omega_s t}, \quad (20)$$

is given by

$$S_{V,a_r}(\tau) = k_6 A e^{-k_5(\tau-k_7)^2} e^{i\omega_s \tau}, \quad (21)$$

where

$$\begin{aligned} k_6 &= k_4 e^{\frac{-D^2}{4\gamma}} \\ k_7 &= \frac{D}{2\gamma}. \end{aligned}$$

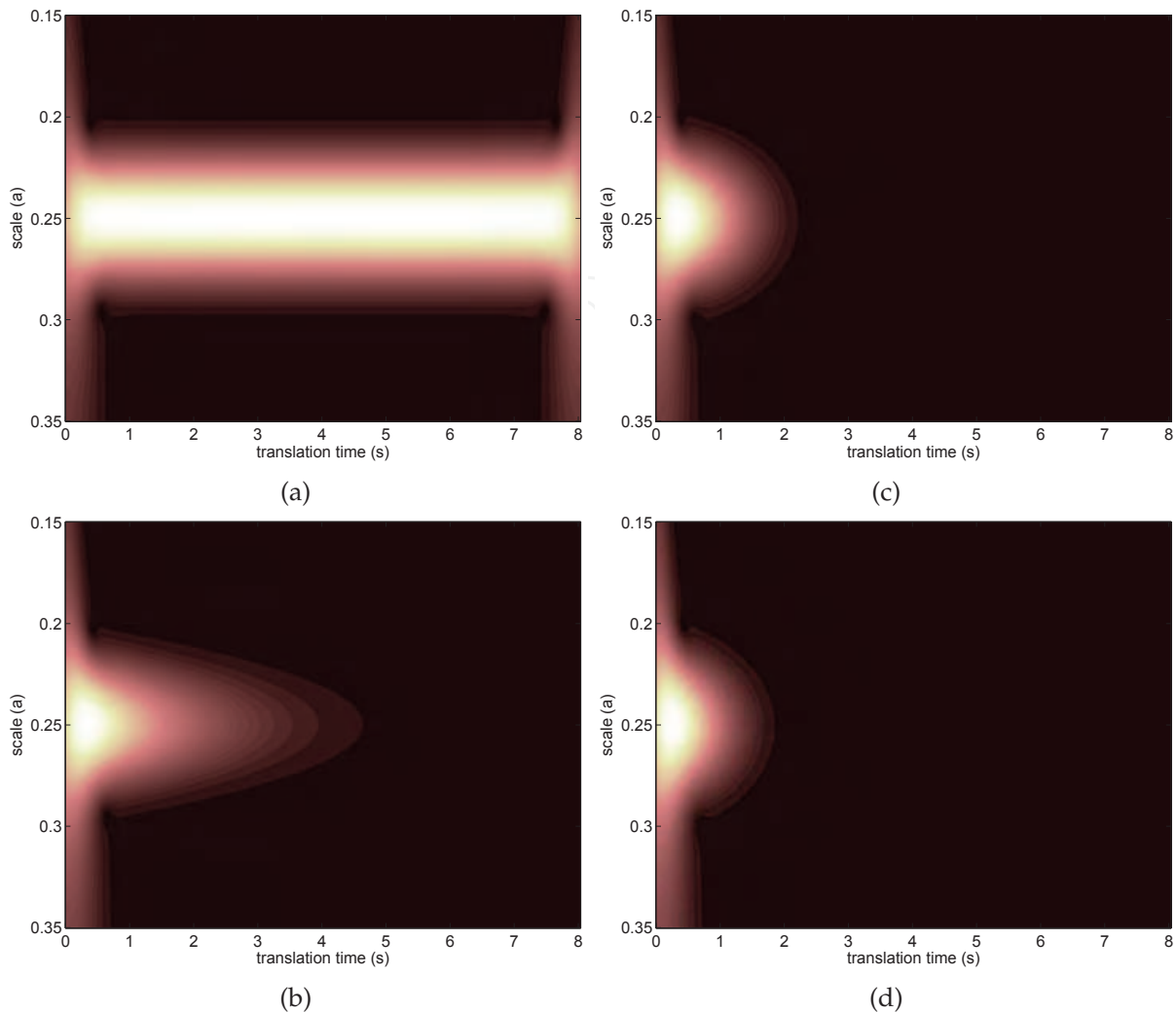


Fig. 12. (a) The modulus of the Morlet WT ($\omega_0 = 15$ rad/s) of a signal of a frequency 60 rad/s with (a) undamped $s(t) = e^{i60t}$; (b) Lorentzian $s(t) = e^{-t}e^{i60t}$; (c) Gaussian $s(t) = e^{-t^2}e^{i60t}$; and (d) Voigt $s(t) = e^{-t}e^{-t^2}e^{i60t}$ lineshape.

That is, at the scale a_r , the Morlet WT of the Voigt lineshape is also a Gaussian function with the same width, but shifted in time, with the amplitude smaller than that of the Gaussian lineshape, and its instantaneous frequency is also equal to ω_s .

Note that the scale $a_r = \omega_0/\omega_s$ does not give exactly the maximum modulus of the WT. However, as seen in Figure 12, the modulus of the Morlet WT of a signal with a Lorentzian lineshape or a Gaussian lineshape (and also a Voigt lineshape) are maximal at the same scale a_r , provided that $a \in \mathbb{R}$ and $\omega_s \gg D$.

Figure 13 shows that the second derivative of the modulus of the Morlet WT can be used to describe the second-order broadening of the lineshape, no matter whether it is Gaussian or Voigt. In the case of a Voigt lineshape, γ actually gives back a Lorentzian whose damping factor is obtained by Eq.(10).

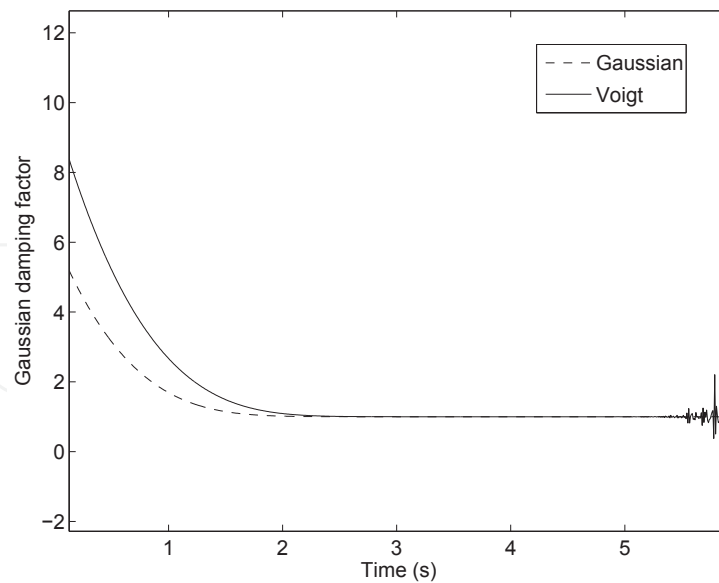


Fig. 13. The Gaussian damping factor derived from the pure Gaussian signal and the Voigt signal considered in Figure 12

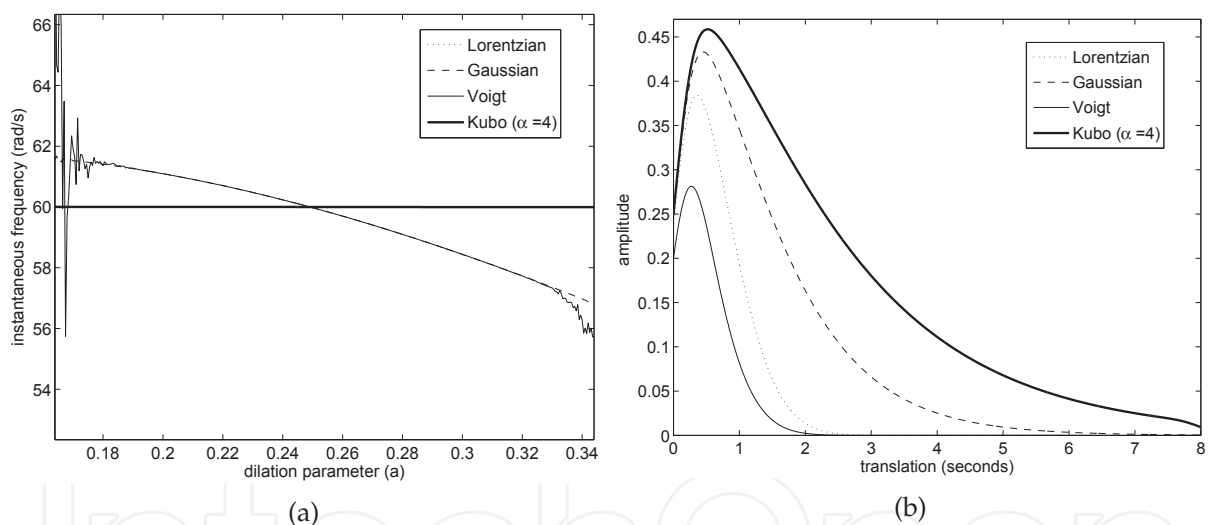


Fig. 14. (a) The comparison of the derived instantaneous frequency of the Morlet WT of a signal of a frequency 60 rad/s with different lineshapes, e.g. Lorentzian $s(t) = e^{-t}e^{i60t}$, Gaussian $s(t) = e^{-t^2}e^{i60t}$, Voigt $s(t) = e^{-t}e^{-t^2}e^{i60t}$ and Kubo $s(t) = e^{-0.25(e^{-t}-1+t)}e^{i60t}$ at $t=4.7$ s. Panel (b) shows the modulus of the Morlet WT of each line at $a_r = \omega_0/60$. Note: $\sigma = 1$, $\omega_0 = 15$ rad/s, $F_s = 800$ s⁻¹, $l = 1024$ points.

Kubo's lineshape

The interaction between the Lorentzian and Gaussian broadening of lineshape depends on the time scale. For example, if the relaxation time (T_2) is much longer than any effect modulating the energy of a molecule, the lineshape will approach the Lorentzian lineshape. On the contrary, if T_2 is short, the lineshape is likely to be Gaussian. In order to account for this time

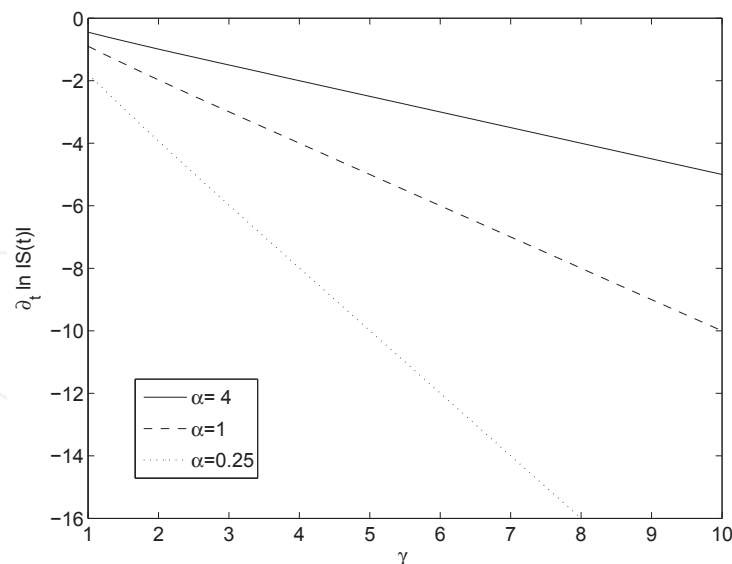


Fig. 15. $\frac{\partial}{\partial \tau} \ln |S_{G,a_r}(\tau)|$ with respect to Kubo's γ for the pure gaussian signal given in Eq.(15), at the scale $a_r = \omega_0/\omega_s$. We have put $\alpha = \gamma/\zeta$, where γ and ζ are the two parameters of the Kubo lineshape defined in Eq.(22).

scale, Kubo (1969) uses a so-called Gaussian-Markovian modulation, namely

$$s(t) = A \exp \left(- \frac{\zeta^2}{\gamma^2} (e^{-\gamma t} - 1 + \gamma t) \right). \quad (22)$$

The parameter γ is inversely proportional to T_2 and ζ is the amplitude of the solvent-induced fluctuations in the frequency. If $\alpha = \gamma/\zeta \ll 1$, the lineshape becomes Gaussian, whereas $\alpha \gg 1$ leads to Lorentzian. The width of the lineshape is $\zeta^2\gamma$.

Solving Eq.(22) seems to be complicated, though may be possible. However, it turns out that the maximum modulus of the Morlet WT of a Kubo lineshape at $\omega_s = 60$ rad/s occurs also at the scale $a_r = \omega_0/\omega_s$, like those of the Gaussian and Lorentzian lineshapes. In addition, the instantaneous frequency is still able to derive the ω_s , even better than the Gaussian lineshape, as shown in Figure 14(a), although the amplitude is broader than those of the Lorentzian, Gaussian or Voigt profiles, as shown in Figure 14(b). The damping parameters can also be derived by the linear relation between $\frac{\partial}{\partial \tau} \ln |S_{G,a_r}(\tau)|$ and γ , as seen in Figure 15, whereas α is related directly to $\frac{\partial^2}{\partial \tau^2} \ln |S_{G,a_r}(\tau)|$.

4. Limitations of the Morlet wavelet transform

In the previous section, the Morlet WT shows its potential for analysing an MRS signal by means of its amplitude and phase, in addition to its time-frequency representation. However, these techniques can be applied to well-defined lineshapes only. Another limitation is the requirement of a proper ω_0 that should distinguish the signal from the solvent, but should not introduce noise in the result. In this section, we will look further on some more limitations that prevent the use of the Morlet WT to quantify MRS signals directly.

4.1 Edge effects

Errors in the wavelet analysis can occur at both ends of the spectrum due to the limited time series. The region of the wavelet spectrum in which effects become important⁵ increases linearly with the scale a , thus it has a conic shape at both ends, as already seen in Figure 1(a) (see also the Appendix). The size of the forbidden region, which is affected by the boundary effect, varies with the frequency ω_0 of the Morlet wavelet function and the ratio between the frequency of the signal (ω_s) and the sampling frequency (F_s). Figure 16 shows that the size becomes larger for a large ω_0 and low ω_s/F_s . In practice, the working region is chosen so that the edge effects are negligible outside and the characterization of the MRS signals should be made inside this region, disregarding the presence of the macromolecular contamination.

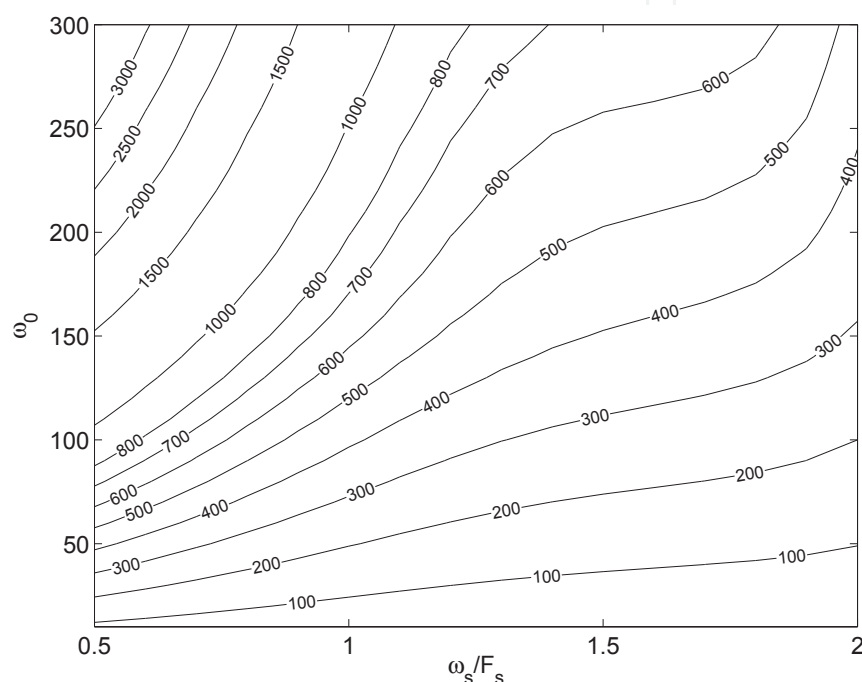


Fig. 16. Lines showing the width (in number of sample points) of the forbidden regions where the boundary effect becomes important, as a function of ω_0 (rad/s) and the ratio between the signal frequency (ω_s) and the sampling frequency (F_s). From (Suvichakorn et al., 2009).

4.2 Interacting/overlapping frequencies

If two frequencies of the signal are close to each other, the wavelet can interact with both of them at the same time. This was already observed in Figure 2(a). Barache et al. (1997) suggested the use of a linear equation system to solve the problem. In the sequel, the simulated N-Acetyl Aspartate (NAA) is used to illustrate how the problem could be solved. The spectrum of the NAA, shown in Figure 17(a), is composed of two different regions, the high, single peak (NAA–acetyl part) and a group of overlapping frequencies (NAA–aspartate part). By using a high ω_0 to separate the overlapping frequencies, the Morlet WT reveals that there are eight frequency peaks in the group as seen in Figure 17(b). The damping factors of the two parts of NAA are shown in Figure 18(a). Applying Eq.(10) directly to each peak causes an oscillation in the derived damping factor, compared to the smooth and stationary damping

⁵ defined as the e -folding time for the autocorrelation of wavelet power at each scale.

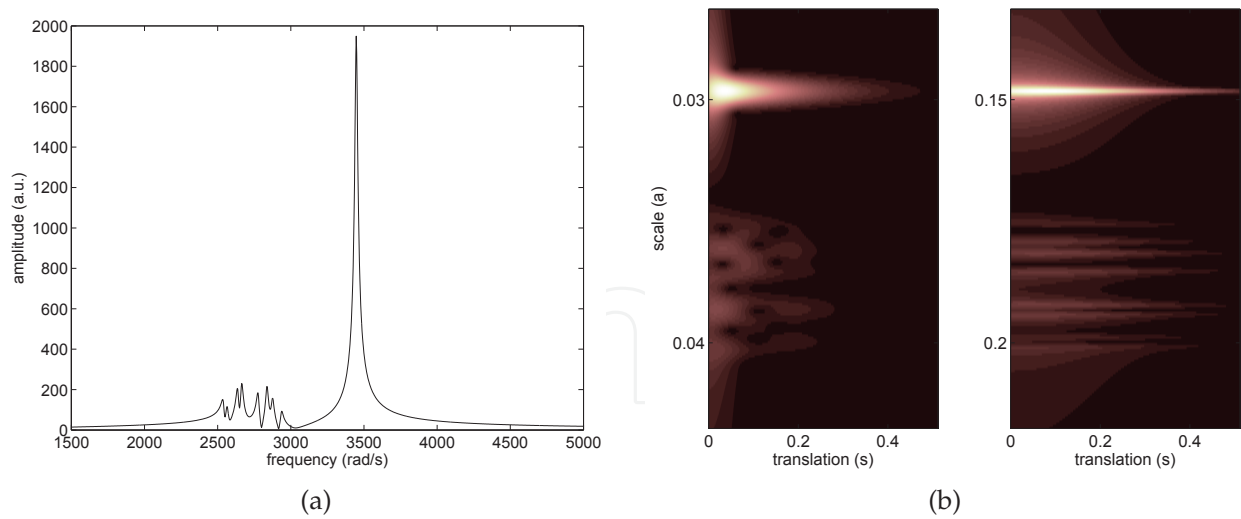


Fig. 17. NAA : (a) Frequency response; (b) Its Morlet wavelet transform for $\omega_0 = 100$ rad/s (left) and $\omega_0 = 500$ rad/s (right). From (Suvichakorn et al., 2009).

factor of the single peak. The size and frequency of the oscillation depends on the numbers of neighbours of each peak and the spectral distance to these neighbours. A proper damping factor can be achieved by averaging these oscillations in time.

Next, we will try to derive the amplitude of each peak. Let us consider an MRS signal composed of n Lorentzian lines $s(t) = e^{-Dt} \sum_n s_n(t)$, where $s_n(t) = A_n e^{i\omega_n t + \varphi_n}$ and $n = 1, 2, \dots$ is an indexing number. Its Morlet WT gives local maxima close to the scales $a_1 = \omega_0/\omega_1$, $a_2 = \omega_0/\omega_2$, and so on. Therefore, we can establish a systematic relation between S_{a_r} and $s_n(t)$ at each scale as follows:

$$\begin{bmatrix} \frac{S_{a_1}(\tau)}{\sqrt{a_1}} \\ \frac{S_{a_2}(\tau)}{\sqrt{a_2}} \\ \frac{S_{a_3}(\tau)}{\sqrt{a_3}} \\ \vdots \end{bmatrix} = \exp(-D\tau) \mathbf{C} \begin{bmatrix} s_1(\tau) \\ s_2(\tau) \\ s_3(\tau) \\ \vdots \end{bmatrix},$$

where $\mathbf{C} = [C_{mn}]$ is a matrix with

$$C_{nn} = \exp\left(\frac{\sigma^2 a_n^2 D^2}{2}\right)$$

$$C_{mn} = \exp\left[-\frac{\sigma^2 \omega_0^2}{2} \left(\frac{\omega_n - \omega_m - iD}{\omega_m}\right)^2\right], \quad m \neq n.$$

The value of $|C_{mn}|$ decreases when the resonating peaks are well resolved (no overlapping frequencies), in fact, it goes to zero when $|\omega_m - \omega_n|$ increases, independently of D . Also, $|C_{mn}|$ decreases when ω_m is high. If C_{mn} is not negligible (overlapping frequencies), solving the linear equations gives the information for each $s_n(t)$.

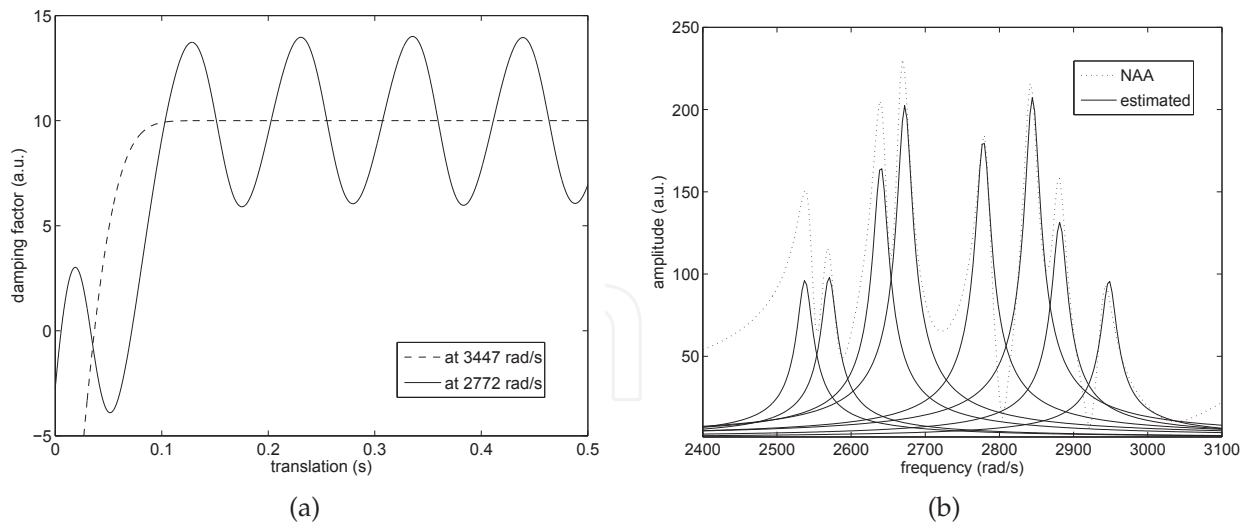


Fig. 18. NAA: (a) Damping function derived by Eq.(10); (b) Amplitudes of NAA–aspartate part, derived by the linear equations (with zero phase). From (Suvichakorn et al., 2009).

The damping parameter D for the equations can be derived by Eq.(10), although the overlapping frequencies may cause oscillations in the solution, but these can be smoothed by averaging in time.

There can be a bias from the estimation, depending on the number and distribution of overlapping frequencies, e.g. the distance between neighbouring frequencies and ω_0 . For the NAA ($\omega = 3447$ rad/s), the bias is approximately 1% of its amplitude (in time domain), when $\omega_0 = 200$ rad/s is used. Note that Lorentzian lineshapes are assumed in these linear equations, and the result is presented in Figure 18(b). In case of non-Lorentzian lineshapes, the arbitrary damping function should be determined, and taken into account to solve the equation.

IntechOpen

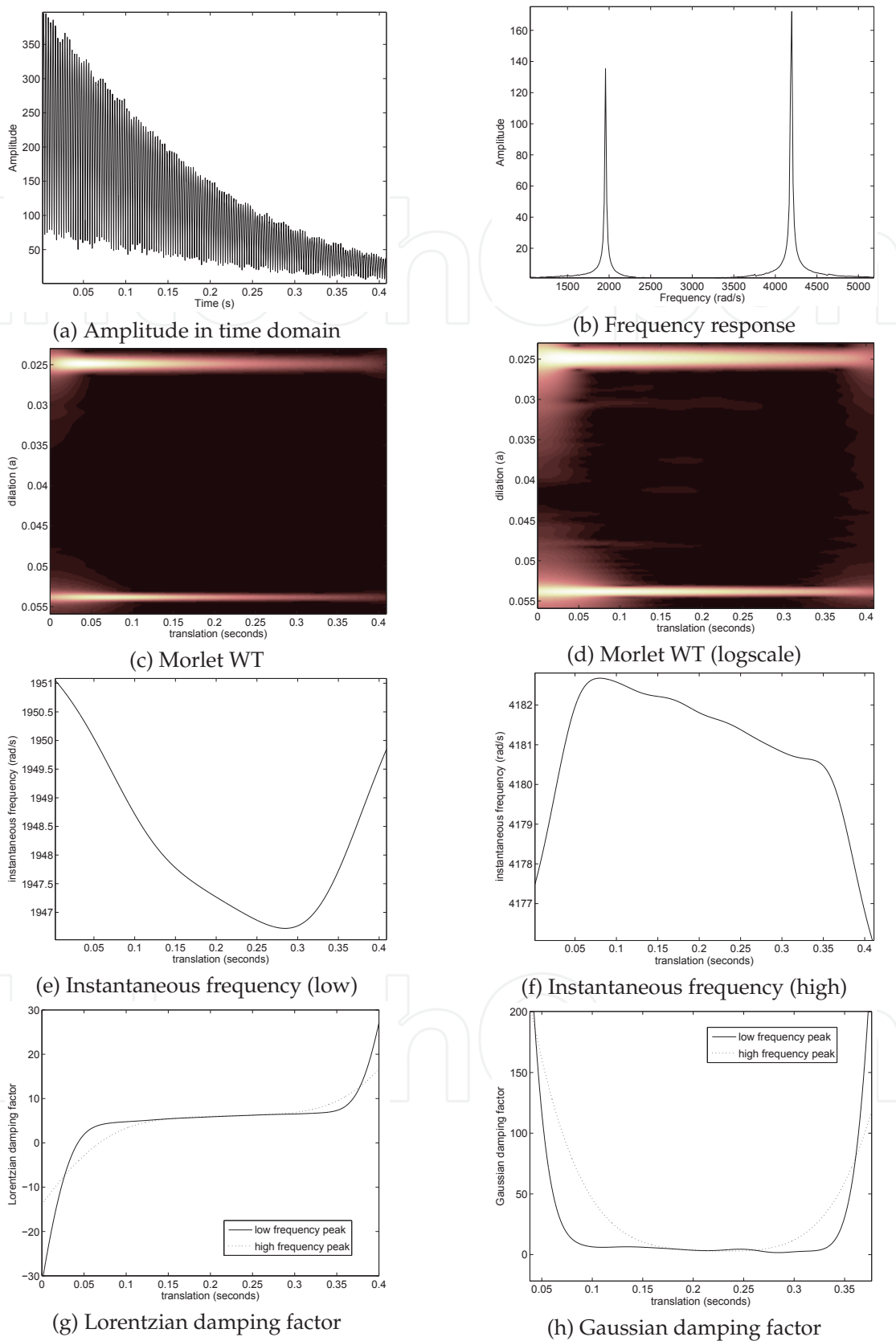


Fig. 19. *In vitro* measured Creatine at 9.4 T

4.3 Arbitrary lineshape

Let us consider a signal with an arbitrary damping function $D(t)$, namely,

$$s(t) = AD(t)e^{i(\omega_s t + \varphi)}. \quad (23)$$

Its Morlet WT is defined by

$$\begin{aligned} S(\tau, a) &= \frac{Ae^{i\varphi}}{2\pi\sigma\sqrt{a}} \int D(t)e^{i\omega_s t} e^{-\frac{1}{2\sigma^2}\left(\frac{t-\tau}{a}\right)^2} e^{-i\omega_0\left(\frac{t-\tau}{a}\right)} dt \\ &= AC_1 \int D(x + \tau) e^{i\omega_s x} e^{-\frac{1}{2\sigma^2}\left(\frac{x}{a}\right)^2} e^{-i\omega_0\left(\frac{x}{a}\right)} dx; \quad x = t - \tau, \\ &= AC_1 \int \mathcal{F}[D(x + \tau)] \mathcal{F}\left[e^{-\frac{x^2}{2\sigma^2 a^2}} e^{-\frac{i(\omega_0 - \omega_s)x}{a}}\right] d\omega \quad (\text{Parseval's theorem}) \\ \frac{1}{\sqrt{a}} S(\tau, a) &= AC_2 \int \mathcal{F}[D(x)] e^{i\tau\omega} e^{-\frac{\omega^2}{2}(a\omega + \omega_s - \omega_0)^2} d\omega, \end{aligned}$$

where $C_1 = \frac{e^{i(\omega_s \tau + \varphi)}}{2\pi\sigma\sqrt{a}}$ and $C_2 = (\sqrt{2\pi})^{-1} e^{i(\omega_s x + \varphi)}$. When implemented (thus discretized), the equation above can be seen as the product of two matrices, namely,

$$\mathbf{S} = C_2 \mathbf{D} \mathbf{G},$$

and the damping function could be solved from the following equations

$$\begin{aligned} A\mathcal{F}[D(x)] &= C_2^{-1} \mathbf{S} \mathbf{G}^{-1}, \\ AD(x) &= C_2^{-1} \mathcal{F}^{-1}[\mathbf{S} \mathbf{G}^{-1}], \\ AD(t) &= C_2^{-1} \mathcal{F}^{-1}[\mathbf{S} \mathbf{G}^{-1} e^{i\tau\omega}], \end{aligned}$$

where \mathbf{S} is the matrix of the scaled wavelet coefficients, \mathbf{G} is derived from the Morlet WT and the frequency-of-interest ω_s , and A is the unknown amplitude of the signal. For a combination of frequencies with the *same* damping function, dividing by $|D(t)|$ should give us a possibility for comparing the amplitude at each peak *relatively*.

5. Working in a real life environment

By real life environment, we mean genuine acquired data, either *in vitro* or *in vivo*, rather than simulated ones. In that case, the ideal Lorentzian lineshape of individual peaks gets distorted. To give an example, we show in Figure 19 the analysis of an *in vitro* creatine signal. We see that intermittent noise appears, in the form of many disrupted, horizontal bands in the WT. Thus the noise occurs for a while at some particular frequencies and then disappears.⁶ Such characteristics differ from the Gaussian white noise that usually appears as vertical bands in the WT. It is also possible that the Gaussian white noise at that duration has the same intensity, however. The analysis of this *in vitro* creatine signal shows that the frequency distribution at each peak is broad and the *almost* stationary Gaussian damping factor indicates that the acquired signal has a lineshape close to that of the Gaussian function. Nevertheless, deriving the amplitude using the Gaussian assumption may lead to an inaccurate estimation.

⁶ We don't know the origin of that noise, which in fact represents the part of the signal that we cannot identify in terms of specific, known contributions.

When the acquisition is made in an *in vivo* environment, the exponential decay of an MRS signal is severely distorted. This is due to the inhomogeneity of the static magnetic field and to eddy currents induced in the magnet walls by switching magnetic gradient fields on and off. Apart from the problem of overlapping frequencies in each metabolite, an *in vivo* MRS signal is composed of several metabolite signatures. Therefore, the challenge is to find a good combination of the amplitudes that the Morlet WT derives at each frequency. Determining complete spectra of each metabolite is preferred to individual resonance. This is yet to be solved.

Appendix: The mathematics of the CWT

A.1. General definitions and properties

The continuous WT is a mathematical tool which permits to decompose a signal in terms of elementary contributions called wavelets. A large body of literature exists for wavelet analysis. We might refer the interested reader to the textbooks of Daubechies (1992), Torr sani (1995), Ali et al. (2000), Antoine et al. (2004), or the elementary introductions (Antoine, 1994) and (Antoine, 2000). These wavelets are obtained from a single function g by translations and dilations,

$$g_{(\tau,a)}(t) = \frac{1}{\sqrt{a}} g\left(\frac{t-\tau}{a}\right), \quad (\text{A.1})$$

where the parameters of translation, $\tau \in \mathbb{R}$, and dilation, $a > 0$, may be continuous or discrete. The CWT of a signal s with the analysing wavelet g is the convolution of s with a scaled and conjugated wavelet $g_a(t) = \overline{g(-t/a)}/a$, where the overbar denotes complex conjugation :

$$S(\tau, a) = g_a * s(\tau) = \frac{1}{\sqrt{a}} \int \overline{g\left(\frac{t-\tau}{a}\right)} s(t) dt. \quad (\text{A.2})$$

It should be remarked that one uses often the so-called L^1 -normalisation, with a factor $1/a$ in (A.1) and (A.2), instead of $1/\sqrt{a}$, in order to enhance small scales, where the finer details lie. In the Fourier domain, the expression (A.2) takes the following form:

$$S(\tau, a) = \frac{1}{2\pi} \int \overline{G(a\omega)} S(\omega) e^{i\omega\tau} d\omega, \quad (\text{A.3})$$

where S and G are the Fourier transforms of the signal s and of the wavelet g , respectively. The equations (A.2) and (A.3) show clearly that the wavelet analysis is a time-frequency analysis, or, more properly, a time-scale analysis (the scale parameter a behaves as the inverse of a frequency). In particular, the relation (A.3) shows that the CWT of a signal s is a filter with a constant relative bandwidth $\Delta\omega/\omega = \text{const}$.

Then a straightforward calculation shows that this transform conserves energy (in the sense of signal processing), that is,

$$\iint |S(\tau, a)|^2 \frac{da d\tau}{a^2} = c_g \int_{-\infty}^{\infty} |s(t)|^2 dt. \quad (\text{A.4})$$

Clearly we must require the wavelet g to satisfy the so-called admissibility condition, namely,

$$c_g \equiv 2\pi \int |G(\omega)|^2 \frac{d\omega}{|\omega|} < \infty. \quad (\text{A.5})$$

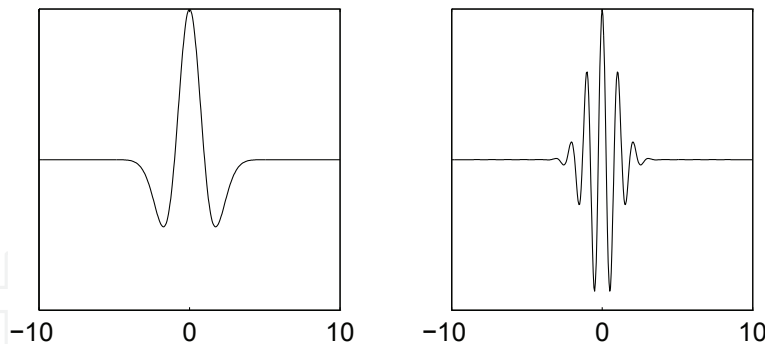


Fig. 20. Two usual one-dimensional wavelets: (left) The Mexican hat or Marr wavelet; (right) The real part of the 1-D Morlet wavelet, for $\omega_0 = 5.6$.

Eq.(A.4) means that the CWT is an isometry from the space of signals onto a closed subspace \mathcal{H}_g of $L^2(\mathbb{R}_+^2, da d\tau/a^2)$, where \mathbb{R}_+^2 denotes the scale-position half-plane $\mathbb{R}_+^2 = \{(\tau, a), \tau \in \mathbb{R}, a > 0\}$. Therefore, the CWT may be inverted on its range \mathcal{H}_g by the adjoint map, and this gives an *exact* reconstruction formula:

$$s(t) = c_g^{-1} \iint g_{(\tau,a)}(t) S(\tau, a) \frac{da d\tau}{a}. \quad (\text{A.6})$$

This formula may also be interpreted as an expansion of the signal into the wavelets $g_{(\tau,a)}$, with (wavelet) coefficients $S(\tau, a)$.

A necessary (and almost sufficient) condition for admissibility is that the wavelet have no DC component:

$$G(0) = 0 \iff \int g(t) dt = 0. \quad (\text{A.7})$$

This is in fact the admissibility condition that is used in practice.

This transform is very general in the sense that there is one CWT for each choice of the analysing wavelet g . For each application, one should select an analysing wavelet adapted to the type of signal at hand. For instance, in order to detect and to characterize the singularities of a signal or a curve, it is advantageous to use as analysing wavelet a derivative of the Gaussian, for instance, the familiar *Mexican hat* (Figure 20, left),

$$g_H(x) = (1 - x^2) e^{-x^2/2} \iff G_H(\omega) = \omega^2 e^{-\omega^2}. \quad (\text{A.8})$$

In our case, MRS signals are relatively well defined in frequency, so it is more interesting to use analysing wavelets which are well localized in frequency space. This is the case of the Morlet wavelet, defined by

$$g_M(t) = e^{i\omega_0 t} e^{-t^2/(2\sigma_0^2)} + h(t) \iff G_M(\omega) = \sqrt{2\pi} \sigma_0 e^{-(\omega - \omega_0)^2 \sigma_0^2 / 2} + H(\omega), \quad (\text{A.9})$$

where the correction term h is necessary to enforce the admissibility condition (in the sequel we shall use the value $\sigma_0 = 1$). If $\omega_0 \sigma_0$ is sufficiently large (typically $\omega_0 \sigma_0 > 5.5$), then h is numerically negligible, and will indeed be omitted. The Morlet wavelet can be interpreted as a bandpass linear filter centered around $\omega = \omega_0/a$ and of weight $1/(\sigma_0 a)$ (Figure 20, right).

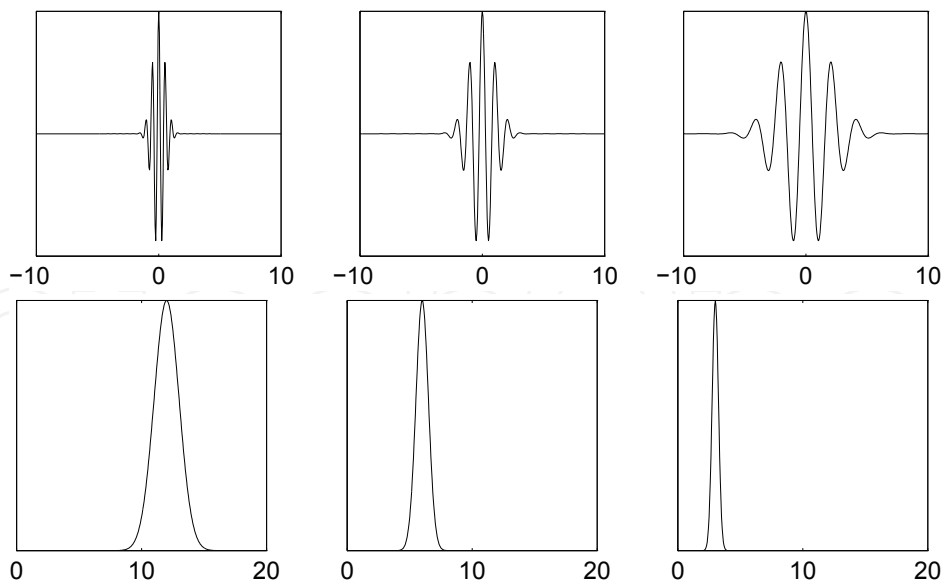


Fig. 21. Support properties of the Morlet wavelet g_M : for $a = 0.5, 1, 2$ (left to right), $g_{(\tau,a)}$ has width 3, 6, 12, respectively (top), while $G_{(\tau,a)}$ has width 3, 1.5, 0.75, and peaks at 12, 6, 3 (bottom).

All the results presented here have been obtained with the Morlet wavelet, but they can easily be generalized to any analysing wavelet whose Fourier transform has a single maximum at $\omega = \omega_0$, or even to the Short Time Fourier Transform (STFT)⁷ (Delprat et al., 1992).

An important fact is the so-called reproduction property. Indeed it may be shown that the orthogonal projection P_g from $L^2(\mathbb{R}_+^2, da d\tau/a^2)$ onto the closed subspace \mathcal{H}_g (the space of wavelet transforms) is an integral operator, with kernel

$$K(\tau', a'; \tau, a) = c_g^{-1} \langle g_{(\tau', a')} | g_{(\tau, a)} \rangle. \quad (\text{A.10})$$

In other words, a function $f \in L^2(\mathbb{R}_+^2, da d\tau/a^2)$ is the WT of some signal if and only if it satisfies the reproduction identity

$$f(\tau', a') = \iint K(\tau', a'; \tau, a) f(\tau, a) \frac{da d\tau}{a^2}. \quad (\text{A.11})$$

For this reason, K is called the *reproducing kernel* of g . It is also the autocorrelation function g and as such it plays an essential role in calibrating the CWT (Antoine, 1994).

Now the relation (A.11) shows that the CWT is enormously redundant (the signal has been unfolded from one variable t to two variables (τ, a)). Thus it is not surprising that the whole information is already contained in a small subset of the values of $S(\tau, a)$. An example of such a subset is the so-called *skeleton*, that is, the set of *ridges*, which are essentially the lines of maxima of the modulus of the WT (in the case of a monochromatic signal, the ridges become horizontal lines $a = a_r$, as we have seen in Section 2). Another example is obtained by taking an appropriate discrete subset $\Gamma = \{a_j, \tau_k\}$ of the half-plane \mathbb{R}_+^2 , as it is necessary in any case

⁷ The STFT is obtained by replacing scaling by modulation in the definition of the wavelets, that is, replacing Eq.(A.1) by $\tilde{g}_{(\tau,a)}(t) = e^{it/a} g(t - \tau)$.

for numerical evaluation of the integrals. However, for most wavelets g , the resulting family $\{g_{(a_j, \tau_k)}\}$ is *never* an orthogonal basis (for the Morlet wavelet, for instance, the kernel K is a Gaussian, thus it never vanishes). At best, it is an overcomplete set of vectors, technically called a *frame*, provided Γ contains sufficiently many points (Daubechies, 1992).

A.2. Localization properties and interpretation

The main virtues of the CWT follow from the support properties of g . Assume g and G to be as well localized as possible (compatible with the Fourier uncertainty principle). More specifically, assume that g has an ‘essential’ support of width L , centered around 0, while G has an essential support of width Ω , centered around ω_0 . Then the transformed wavelets $g_{(\tau, a)}$ and $G_{(\tau, a)}$ have, respectively, an essential support of width aL around τ and an essential support of width Ω/a around ω_0/a . This behavior is illustrated in Figure 21, which shows the Morlet wavelet in the time and frequency domains, for three successive scales $a = 0.5, 1$ and 2 , from left to right. Notice that the product of the two widths is constant (we know it has to be bounded below by a fixed constant, by the (Fourier) uncertainty principle). Remember that $1/a$ behaves like a frequency. Therefore:

- if $a \gg 1$, $g_{(\tau, a)}$ is a wide window, whereas $G_{(\tau, a)}$ is very peaked around a small frequency ω_0/a : this transform is most sensitive to *low frequencies*.
- if $a \ll 1$, $g_{(\tau, a)}$ is a narrow window and $G_{(\tau, a)}$ is wide and centered around a high frequency ω_0/a : this wavelet has a good localization capability in the space domain and is mostly sensitive to *high frequencies*.

Combining now these localization properties with the zero mean condition and the fact that $g_{(\tau, a)}$ acts like a filter (convolution), we see that the CWT performs a *local filtering*, both in time and in scale. The WT $S(\tau, a)$ is nonnegligible only when the wavelet $g_{(\tau, a)}$ matches the signal $s(t)$, that is, it filters the part of the signal, if any, that lives around the time τ and the scale a . Taking all these properties together, one is naturally led to the interpretation of the CWT as a *mathematical microscope*, with optics g , position τ and global magnification $1/a$. In addition, the analysis works at constant relative bandwidth ($\Delta\omega/\omega = \text{constant}$), so that it has a better resolution at high frequency, i.e., small scales. This property makes it an ideal tool for detecting *singularities* (for instance, discontinuities in the signal or one of its derivatives), and also scale dependent features, in particular, for analysing *fractals*.

A.3. Implementation questions

Faced with this new tool, one must begin by learning the rules of the trade, that is, one must learn how to read and understand a CWT (Grossmann et al., 1990). The simplest way is to get some practice on very simple academic signals, such as a simple discontinuity in time or a monochromatic signal (pure sinusoid). We note that it is natural to use a logarithmic scale for the scale parameter a . The visual effect is that the lines, $\tau/a = \text{constant}$, are not straight lines, but hyperbolic curves; at the same time, the horizon $a = 0$ recedes to infinity (see Figure 22). The analysing wavelet g is supposed to be complex, so that we may treat separately the modulus and the phase of the transform. The scale axis, in units of $\ln a$, points downward, so that high frequencies (small a) correspond to the top of the plots, and low frequencies (large a) to the bottom. The results are presented by coding the height of the function by density of points (12 levels of gray, from white to black). The phase is 2π -periodic. When it reaches 2π , it is wrapped around to the value 0. Thus the lines of constant phase with value $2k\pi$ are lines of discontinuity, where the density of points drops abruptly from 1 (black) to 0 (white). In

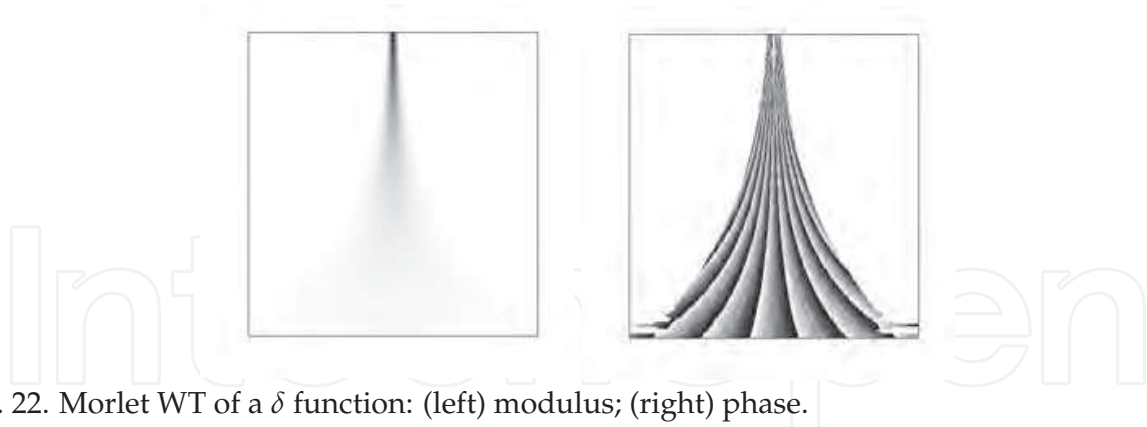


Fig. 22. Morlet WT of a δ function: (left) modulus; (right) phase.

addition, the functions plotted are thresholded at 1% of the maximum value of the modulus of $S(\tau, a)$. We will now analyse the two academic signals mentioned above.

(i) *A simple discontinuity*

The simplest signal is a simple discontinuity in time, at $t = t_0$, modelled by $s(t) = \delta(t - t_0)$. The WT is obtained immediately and reads

$$S(\tau, a) = a^{-1/2} \overline{g(a^{-1}(t_0 - \tau))}. \quad (\text{A.12})$$

The following features may be read off Eq.(A.12):

- The phase of $S(\tau, a)$ is constant on the lines $\tau/a = \text{constant}$, originating from the point $\tau = t_0$ on the horizon. These lines point towards the position of the singularity, like a finger.
- On the same lines of constant phase, the modulus of $S(\tau, a)$ increases as $a^{-1/2}$ when $a \rightarrow 0$, so that the singularity is enhanced. The effect is even more pronounced if one uses the L^1 normalisation.

This is illustrated on Figure 22, which presents the modulus and phase of the WT of a δ function, using a standard Morlet wavelet (but the result is independent of the choice of g).

The interesting point is that this behavior is extremely robust. For instance, the 'finger' pointing to a δ -singularity remains clearly visible when the latter is superposed on a continuous signal (even if the amplitude of the δ function is too small to be invisible on the signal itself), or even in the presence of substantial background noise. Similarly, the discontinuity corresponding to the abrupt onset of a signal is readily identified with the CWT. We refer to (Grossmann et al., 1990) for several spectacular examples.

This is the origin of the *edge* or *boundary effects* that we have encountered in Section 4.1. The first notion is that of cone of confidence or *cone of influence*. Let the wavelet g vanish outside the interval $I_g = [t_{\min}, t_{\max}]$. Then, given a point t_0 in the support of the signal, the region in which it influences the WT is the cone $\tau \in aI_g + t_0 = [-at_{\min} + t_0, at_{\max} + t_0]$. Thus the region of influence increases linearly with a . The effect is clearly seen in Figure 1: the cones of influence of the two endpoints of the spectrum are the regions where the phase of the WT differs from that of a pure sinusoid (see (ii) below). This is the region to be avoided, as discussed in Section 4.1.

(ii) *A single monochromatic wave*

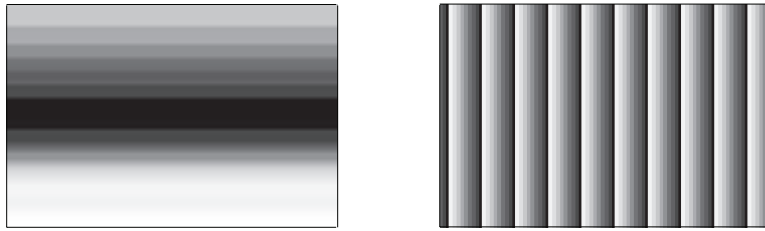


Fig. 23. Morlet WT of a single sinusoid: (left) modulus; (right) phase.

Equally simple is a single harmonic signal (monochromatic wave):

$$s(t) = e^{i\omega_s t} \Leftrightarrow S(\omega) = \frac{1}{\sqrt{2\pi}} \delta(\omega - \omega_s), \quad (\text{A.13})$$

which gives

$$S(\tau, a) = \sqrt{\frac{a}{2\pi}} G(a\omega_s) e^{i\omega_s \tau} = S(a, 0) e^{i\omega_s \tau}. \quad (\text{A.14})$$

The same relations remain true for a real monochromatic signal, $s(t) = \sin \omega_s t$ or $s(t) = \cos \omega_s t$, if the wavelet g is progressive (that is, $G(\omega) = 0$ for $\omega \leq 0$).

Again two important properties may be read off immediately from Eq.(A.14):

- The modulus of $S(\tau, a)$ is independent of τ . Hence, the graph of $|S(\tau, a)|$ consists of horizontal bands and the profile for a fixed time τ essentially reproduces the profile of G .
- The phase of $S(\tau, a)$ is linear in τ . Since the phase is 2π -periodic, the graph of $\Phi(\tau, a) := \arg S(\tau, a)$ is a linear sawtooth function:

$$\Phi(\tau, a) = \omega_s \tau \pmod{2\pi}. \quad (\text{A.15})$$

These properties are illustrated on Figure 23 for a single sine function analysed with a Morlet wavelet. This pattern of equidistant vertical black-to-white bands is the signature of a pure frequency signal. This can be seen already in Figure 1.

Both the modulus and the phase allow to determine the frequency ω_s of the signal. If the modulus of the wavelet $G(\omega)$ has a single maximum for $\omega = \omega_0$, Eq.(A.14) gives immediately $\omega_s = \omega_0/a_r$, where a_r is the scale corresponding to the maximum in the profile of $|S(\tau, a)|$ for fixed τ . For instance, the (truncated) Morlet wavelet $g(t) = \exp(i\omega_0 t) \exp(-t^2/2)$ yields:

$$S(\tau, a) = \sqrt{a} e^{-\frac{1}{2}(a\omega_s - \omega_0)^2} e^{i\omega_s \tau}, \quad (\text{A.16})$$

and the result is obvious. As for the phase, Eq.(A.15) gives, at least locally:

$$\frac{\partial \Phi(\tau, a)}{\partial \tau} = \omega_s = \frac{\omega_0}{a_r}. \quad (\text{A.17})$$

A.4. The discrete wavelet transform

Notice that the discretized CWT which is used in practice, including in the present text, is totally different from the so-called *discrete WT* (DWT). Indeed, orthogonal bases of wavelets may be constructed, but from a completely different approach based on the notion of *multiresolution analysis*.

We emphasize that the DWT is totally different in spirit from the CWT, either truly continuous or discretized, and they have complementary ranges of applications:

- In the CWT, there is a lot of freedom in choosing the wavelet g , but one does not get an orthonormal basis, at best a frame. This is a tool for analysis and feature determination, as in MRS or other problems where the scaling properties of the signal are unknown *a priori*, for instance in fractal analysis.
- In the DWT, one insists on having an orthonormal basis, but the wavelet is *derived* from the multiresolution analysis. This is the preferred tool for data compression and signal synthesis, and the most popular in the signal processing community.

More radically, one may even say that the kind of problems treated here can be solved only with the CWT, the DWT is simply not adapted to the underlying physics, although it has been proposed for MRS (Neue, 1996). For instance, the algorithm for detecting spectral lines, as well as the ridge concept, rest upon a stationary phase argument. Similarly, the determination of fractal exponents exploits the scaling behaviour of homogeneous functions or distributions and the covariance properties of the CWT. All these notions are foreign to the DWT, which is more a signal processing tool.

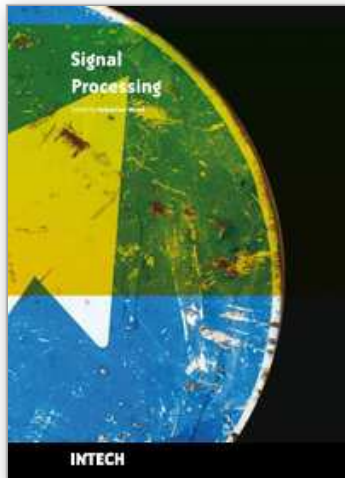
6. References

- Ali, S. T., Antoine, J.-P. & Gazeau, J.-P. (2000). *Coherent States, Wavelets and Their Generalizations*, Springer-Verlag, New York, Berlin, Heidelberg.
- Antoine, J.-P. (1994). Wavelet analysis: A new tool in signal processing, *Physica Mag.* **16**: 17–42.
- Antoine, J.-P. (2000). Wavelet analysis of signals and images, a grand tour, *Revista Ciencias Matematicas (La Habana)* **18**: 113–143.
- Antoine, J.-P., Murenzi, R., Vandergheynst, P. & Ali, S. T. (2004). *Two-Dimensional Wavelets and their Relatives*, Cambridge University Press, Cambridge (UK).
- Barache, D., Antoine, J.-P. & Dereppe, J.-M. (1997). The continuous wavelet transform, an analysis tool for NMR spectroscopy, *Journal of Magnetic Resonance* **128**: 1–11.
- Behar, K. L., Rothman, D. L., Spencer, D. D. & Petroff, O. A. C. (1994). Analysis of macromolecule resonances in ^1H NMR spectra of human brain, *Magnetic Resonance in Medicine* **32**(3): 294–302.
- Cudalbu, C., Beuf, O. & Cavassila, S. (2009). *In vivo* short echo time localized ^1H MRS of the rat brain at 7 T: influence of two strategies of background accommodation on the metabolite concentration estimation using QUEST, *J. Sign. Process. Syst.* **55**: 25–34.
- Cudalbu, C., Bucur, A., Graveron-Demilly, D., Beuf, O. & Cavassila, S. (2007). Comparison of two strategies of background-accommodation: Influence on the metabolite concentration estimation from *in vivo* magnetic resonance spectroscopy data, *Proceedings of the 29th IEEE EMBC*, pp. 2077–2080.
- Cudalbu, C., Cavassila, S., Rabeson, H., van Ormondt, D. & Graveron-Demilly, D. (2008). A comparison between the influence of *in vitro* and simulated basis-sets on estimated metabolite concentrations, *NMR in Biomedicine* **21**: 627–636.

- Daubechies, I. (1992). *Ten Lectures on Wavelets*, SIAM, Philadelphia.
- Delprat, N., Escudié, B., Guillemain, P., Kronland-Martinet, R., Tchamitchian, P. & Torrèsani, B. (1992). Asymptotic wavelet and Gabor analysis extraction of instantaneous frequencies, *IEEE Transactions on Information Theory* **38**(2): 644–664.
- Devos, A., Lukas, L., Suykens, J. A. K., Vanhamme, L., Tate, A. R., Howe, F. A., Majos, C., Moreno-Torres, A., Arus, C., der Graaf, M. V. & Huffel, S. V. (2004). Recent advances in magnetic resonance neurospectroscopy, *Journal of Magnetic Resonance* **170**: 164–175.
- Franzen, S. (2002). *Lecture Notes on Molecular Spectroscopy*, Department of Chemistry, NC State University. <http://chsfpc5.chem.ncsu.edu/franzen/CH795Z/>.
- Govindaraju, V., Young, K. & Maudsley, A. A. (2000). Proton NMR chemical shifts and coupling constants for brain metabolites., *NMR in Biomedicine* **13**: 129–153.
- Grossmann, A., Kronland-Martinet, R. & Morlet, J. (1990). Reading and understanding continuous wavelet transforms, in J.-M. Combes, A. Grossmann & P. Tchamitchian (eds), *Wavelets, Time-Frequency Methods and Phase Space (Proc. Marseille 1987)*, 2d ed., Springer-Verlag, Berlin, pp. 2–20.
- Guillemain, P., Kronland-Martinet, R. & Martens, B. (1992). Estimation of spectral lines with the help of the wavelet transform, applications in NMR spectroscopy, in Y. Meyer (ed.), *Wavelets and applications— Proc. Int. Conf. Marseille, France, May 1989*, Masson, Paris, and Springer, Berlin, pp. 38–60.
- Hornak, J. P. (1997). *The Basics of NMR*, Department of Chemistry, Rochester Institute of Technology, Rochester, NY. <http://www.cis.rit.edu/htbooks/nmr/>.
- Jacques, L., Coron, A., Vandergheynst, P. & Rivoldini, A. (2007). The YAWTb toolbox : Yet Another Wavelet Toolbox. <http://rhea.tele.ucl.ac.be/yawtb>.
- Kubo, R. (1969). A stochastic theory of line shape, *Advances in Chemical Physics: Stochastic Processes in Chemical Physics* **15**: 101–127.
- Mainardi, L. T., Origgi, D., Lucia, P., Scotti, G. & Cerutti, S. (2002). A wavelet packets decomposition algorithm for quantification of in vivo 1H-MRS parameters, *Medical Engineering & Physics* **24**(3): 201–208.
- Marshall, I., Bruce, S. D., Higinbotham, J., MacLulich, A., Wardlaw, J. M., Ferguson, K. J. & Seckl, J. (2000). Choice of spectroscopic lineshape model affects metabolite peak areas and area ratios, *Magnetic Resonance in Medicine* **44**: 646–649.
- Mierisová, S. & Ala-Korpela, M. (2001). MR spectroscopy quantitation: a review of frequency domain methods, *NMR in Biomedicine* **14**(4): 247–259.
- Neue, G. (1996). Simplification of dynamical NMR spectroscopy by wavelet transform, *Solid State Nuclear Magnetic Resonance* **5**: 305–314.
- Pijnappel, W. W. F., van den Boogaart, A., de Beer, R. & van Ormondt, D. (1992). SVD-based quantification of magnetic resonance signals, *Journal of Magnetic Resonance* **97**(11): 122–134.
- Poulet, J. B., Sima, D. M., Simonetti, A. W., Neuter, B. D., Vanhamme, L., Lemmerling, P. & Huffel, S. V. (2007). An automated quantitation of short echo time MRS spectra in an open source software environment: AQSES, *NMR in Biomedicine* **20**: 493–504.
- Provencher, S. W. (1993). Estimation of metabolite concentrations from localized in vivo proton NMR spectra, *Magnetic Resonance in Medicine* **30**: 672–679.
- Rabeson, H., Ratiney, H., Cudalbu, C., Cavassila, S., Capobianco, E., de Beer, R., van Ormondt, D. & Graveron-Demilly, D. (2006). Signal disentanglement in in vivo MR spectroscopy by semi-parametric processing or by measurement?, *Proceedings of the*

- Annual Workshop on Circuits, Systems and Signal Processing (ProISC)*, IEEE Benelux, The Netherlands, pp. 176–183.
- Ratiney, H., Bucur, A., Sdika, M., Beuf, O., Pilleul, F. & Cavassila, S. (2008). Effective Voigt model estimation using multiple random starting values and parameter bounds settings for *in vivo* hepatic ¹H magnetic resonance spectroscopy data, *Proc. ISBI*, Paris, pp. 1529–1532.
- Ratiney, H., Coenradie, Y., Cavassila, S., van Ormondt, D. & Graveron-Demilly, D. (2004). Time-domain quantitation of short echo-time signals: background accommodation, *Magn. Reson. Mater. Phy.* **16**: 284–296.
- Ratiney, H., Sdika, M., Coenradie, Y., Cavassila, S., van Ormondt, D. & Graveron-Demilly, D. (2005). Time-domain semi-parametric estimation based on a metabolite basis set, *NMR in Biomedicine* **18**: 1–13.
- Serrai, H., Senhadji, L., de Certaines, J. D. & Coatrieux, J. L. (1997). Time-domain quantification of amplitude, chemical shift, apparent relaxation time t_2^* , and phase by wavelet-transform analysis. application to biomedical magnetic resonance spectroscopy, *Journal of Magnetic Resonance* **24**: 20–34.
- Suvichakorn, A., Ratiney, H., Bucur, A., Cavassila, S. & Antoine, J.-P. (2009). Toward a quantitative analysis of *in vivo* proton magnetic resonance spectroscopic signals using the continuous Morlet wavelet transform, *Meas. Sci. Technol.* p. Technol. 20: paper # 104029.
- Torrésani, B. (1995). *Analyse continue par ondelettes*, InterEditions & CNRS Editions, Paris.
- Vanhamme, L., Sundin, T., Hecke, P. V. & Huffel, S. V. (2001). MR spectroscopic quantitation: A review of time domain methods, *NMR in Biomedicine* **14**(4): 233–246.
- Vanhamme, L., van den Boogaart, A. & Huffel, S. V. (1997). Improved method for accurate and efficient quantification of MRS data with use of prior knowledge, *Journal of Magnetic Resonance* **12**: 35–43.

IntechOpen



Signal Processing

Edited by Sebastian Miron

ISBN 978-953-7619-91-6

Hard cover, 528 pages

Publisher InTech

Published online 01, March, 2010

Published in print edition March, 2010

This book intends to provide highlights of the current research in signal processing area and to offer a snapshot of the recent advances in this field. This work is mainly destined to researchers in the signal processing related areas but it is also accessible to anyone with a scientific background desiring to have an up-to-date overview of this domain. The twenty-five chapters present methodological advances and recent applications of signal processing algorithms in various domains as telecommunications, array processing, biology, cryptography, image and speech processing. The methodologies illustrated in this book, such as sparse signal recovery, are hot topics in the signal processing community at this moment. The editor would like to thank all the authors for their excellent contributions in different areas of signal processing and hopes that this book will be of valuable help to the readers.

How to reference

In order to correctly reference this scholarly work, feel free to copy and paste the following:

A. Suvichakorna, H. Ratiney, S. Cavassila and J.-P Antoine (2010). Wavelet-based Techniques in MRS, Signal Processing, Sebastian Miron (Ed.), ISBN: 978-953-7619-91-6, InTech, Available from: <http://www.intechopen.com/books/signal-processing/wavelet-based-techniques-in-mrs>

INTECH
open science | open minds

InTech Europe

University Campus STeP Ri
Slavka Krautzeka 83/A
51000 Rijeka, Croatia
Phone: +385 (51) 770 447
Fax: +385 (51) 686 166
www.intechopen.com

InTech China

Unit 405, Office Block, Hotel Equatorial Shanghai
No.65, Yan An Road (West), Shanghai, 200040, China
中国上海市延安西路65号上海国际贵都大饭店办公楼405单元
Phone: +86-21-62489820
Fax: +86-21-62489821

© 2010 The Author(s). Licensee IntechOpen. This chapter is distributed under the terms of the [Creative Commons Attribution-NonCommercial-ShareAlike-3.0 License](https://creativecommons.org/licenses/by-nc-sa/3.0/), which permits use, distribution and reproduction for non-commercial purposes, provided the original is properly cited and derivative works building on this content are distributed under the same license.

IntechOpen

IntechOpen